Outer membrane lipoprotein DolP interacts with the BAM complex and promotes fitness during envelope stress response

David Ranava[1,§], Yiying Yang[1,§], Luis Orenday-Tapia[1,§], François Rousset[2], Catherine Turlan[1], Lun Cui[2], Violette Morales[1], Cyril Moulin[1], Gladys Munoz[1], Jérôme Rech[1], Anne Caumont-Sarcos[1], Cécile Albenne[1], David Bikard[2], Raffaele Ieva[1*]

[1]Laboratoire de Microbiologie et Génétique Moléculaires (LMGM), Centre de Biologie Intégrative (CBI), Université de Toulouse, CNRS, UPS, Toulouse 31062, France.

[2]Synthetic Biology Group, Microbiology Department, Institut Pasteur, Paris 75015, France.

[§]These authors contributed equally to this paper.

*Correspondance to:

Raffaele Ieva, raffaele.ieva@univ-tlse3.fr

Abstract

In Gram-negative bacteria, coordinated remodelling of the outer membrane (OM) and the peptidoglycan is crucial for envelope integrity. Envelope stress caused by unfolded OM proteins (OMPs) activates sigmaE (σ^E) in Enterobacteria. σ^E upregulates OMP biogenesis factors, including the β-barrel assembly machinery (BAM) that catalyzes OMP-folding. Elevated σ^E activity, however, can be detrimental for OM integrity. Here we report that DolP (YraP), a σ^E-upregulated OM lipoprotein important for envelope integrity, is a novel interactor of BAM and we demonstrate that OM-assembled BamA is a critical determinant of the BAM-DolP complex. Mid-cell recruitment of DolP had been previously associated to activation of septal peptidoglycan remodelling during cell division, but its role during envelope stress was unknown. We now show that DolP promotes cell fitness upon stress-induced activation of σ^E and opposes a detrimental effect caused by the overaccumulation of BAM in the OM. During envelope stress, DolP loses its association with the mid-cell, thus suggesting a possible link between envelope stress caused by impaired OMP biogenesis and the regulation of a late step of cell division.

Introduction

The outer membrane (OM) of Gram-negative bacteria forms a protective barrier against harmful compounds, including several antimicrobials. This envelope structure surrounds the inner membrane and the periplasm that contains the peptidoglycan, a net-like structure made of glycan chains and interconnecting peptides. During cell division, the multi-layered envelope structure is remodelled by the divisome machinery [1]. At a late step of division, septal peptidoglycan synthesized by the divisome undergoes splitting, initiating the formation of the new poles of adjacent daughter cells. Finally, remodelling of the OM barrier completes formation of the new poles in the cell offspring. The mechanisms by which cells coordinate OM remodelling with peptidoglycan splitting, preserving the permeability barrier of this protective membrane, are ill-defined [2].

Integral outer membrane proteins (OMPs) are crucial to maintain the OM permeability barrier. OMPs fold into amphipathic β-barrel structures that span the OM and carry out a variety of tasks. Porins are OMPs that facilitate the diffusion of small metabolites. Other OMPs function as cofactor transporters, secretory channels, or machineries for the assembly of proteins and lipopolysaccharide (LPS) [3,4], a structural component of the external OM leaflet that prevents the diffusion of noxious chemicals [4]. The β-barrel assembly machinery (BAM) is a multi-subunit complex that mediates the folding and membrane insertion of OMPs transiting through the periplasm [5,6]. The essential and evolutionarily conserved BamA insertase subunit is an OMP consisting of an amino (N)-terminal periplasmic domain made of polypeptide transport-associated (POTRA or P) motifs and a carboxy (C)-terminal 16-stranded β-barrel membrane domain that catalyzes OMP biogenesis [7,8]. The flexible pairing of β-strands 1 and 16 of the BamA β-barrel controls a lateral gate connecting the interior of the barrel towards the surrounding lipid bilayer [9-12].

68 Conformational dynamics of the BamA β-barrel region proximal to the lateral gate is
69 thought to locally increase the entropy of the surrounding lipid bilayer [9,13,14] and
70 assist the insertion of nascent OMPs into the OM [11,15,16]. The N-terminal periplasmic
71 portion of BamA from the enterobacterium *Escherichia coli* contains five POTRA
72 motifs that serve as a scaffold for four lipoproteins, BamBCDE, which assist BamA
73 during OMP biogenesis [17-19]. The N-terminal POTRA motif is also the docking site of
74 the periplasmic chaperone SurA [20]. Together with the chaperones Skp and DegP,
75 SurA contributes to monitor unfolded OMPs transported into the periplasm by the
76 inner membrane general secretory (Sec) pathway [21,22].

77 Defective OMP assembly causes periplasmic accumulation of unfolded
78 protein transport intermediates. This envelope stress is signalled across the inner
79 membrane to induce the sigmaE (σ^E)-mediated transcriptional response [23]. In the
80 absence of stress, σ^E is sequestered by the inner membrane-spanning RseA factor.
81 By-products of misfolded OMP turnover activate degradation of RseA, liberating σ^E
82 [24]. The σ^E response copes with stress i) by upregulating genes involved in OMP
83 biogenesis, such as the *bam* genes [25], and ii) by lowering the OMP biogenesis
84 burden via a post-transcriptional mechanism [26]. Whereas σ^E is essential [27], a tight
85 control of cytosolic σ^E availability is necessary for optimal cell fitness and to prevent
86 a potentially detrimental effect on the envelope [28-31]. Remarkably, the functions of a
87 number of genes upregulated by σ^E remains unknown. Among those, *yraP* encodes
88 a ~20 kDa OM-anchored lipoprotein largely conserved in γ and β proteobacteria [32-
89 36]. YraP is crucial for OM integrity [34] and pathogenicity [32]. A recent study showed
90 that YraP localizes at the mid-cell during a late step of cell division, where it
91 contributes to the regulation of septal peptidoglycan splitting by an unknown
92 mechanism [33]. These observations do not explain why YraP is upregulated in
93 response to σ^E activation and how YraP helps coping with envelope stress.

94 During cell division, envelope stress caused by defective OMP biogenesis
95 would place an additional burden on the already-complicated envelope reshaping

process faced by cells. It remains unknown whether stress caused by unfolded OMPs influences envelope remodelling at the forming poles of two adjacent daughter cells. Here we present a functional investigation of *yraP* prompted by a genome-wide synthetic-defect screen. We demonstrate genetic interactions of *yraP* with *bam* genes and we provide evidence that YraP can associate with the BAM complex via an interaction with the BamA subunit. YraP is not critical for OMP assembly but promotes fitness upon activation of the σ^E response. Upon envelope stress or when BAM overaccumulates in the OM, YraP loses its association with the mid-cell, thus suggesting a possible link between the envelope stress response and septal peptidoglycan hydrolysis during a late step of cell division. Hence, we propose to rename YraP as DolP (division- and OM stress-associated lipoprotein).

107 **Results**

108

109 **A genome-wide synthetic-defect screen identifies *dolP* genetic interactions**

110 The mutant allele Δ*dolP::kan* [37] was introduced into *E. coli* BW25113 by P1
111 transduction. The resulting Δ*dolP* strain grew normally on LB medium (Figs. S1A
112 and S1B), but was highly susceptible to vancomycin (Figs. 1A and S1B). This
113 antibiotic is normally excluded from the OM of wild-type cells but inhibits growth of
114 cells lacking OMP biogenesis factors such as *skp* and *surA* (Fig. S1B). The
115 expression of C-terminally fused DolP protein variants in place of its wild-type form
116 restored vancomycin resistance (Fig. 1A and Fig. S1C). This result supports the
117 notion that DolP is important for envelope integrity [33-36]. However, the role of DolP
118 during envelope stress remains poorly understood.

119 A previous study showed that lack of DolP causes a severe growth defect in
120 a *surA* deletion strain, however the cause of this synthetic phenotype has remained
121 unclear [34]. To gain insights into the role of DolP, we subjected Δ*dolP* cells to a
122 genome-wide synthetic-defect screen exploiting a Clustered Regularly Interspersed
123 Short Palindromic Repeat interference (CRISPRi) approach. Targeting of the
124 catalytically inactive dCas9 nuclease by gene-specific single guides RNAs
125 (sgRNAs) enables gene repression (Fig. 1B) [38]. The EcoWG1 sgRNA library
126 targeting the entire genome of *E. coli* MG1655 [39] was introduced into isogenic Δ*dolP*
127 or *dolP*$^{+}$ MG1655-derivative strains. The fitness of each knockdown was then
128 compared in these backgrounds by deep-sequencing of the sgRNA library after ~17
129 growth generations. The outputs obtained from two independent tests were highly
130 reproducible (Fig. S2A). A strong fitness defect in the Δ*dolP* strain was caused by
131 the targeting of *envC* (Fig. 1C, Fig. S2B and Tables S1 and S2), followed by the
132 targeting of *ftsX* and *ftsE* (Fig. 1C, Tables S1 and S2). A validation growth test
133 showed that the synthetic fitness defect observed for Δ*dolP* cells was caused by
134 dCas9-dependent silencing of *ftsX* and *envC* (Fig. 1D, panels 6 and 7). The ABC

135 transporter-like complex FtsE/FtsX has multiple roles in organizing the cell
136 divisome, including the recruitment of periplasmic EnvC, a LytM domain-containing
137 factor required for the activation of amidases that hydrolyse septal peptidoglycan [40].
138 This peptidoglycan remodelling reaction is mediated by two sets of highly controlled
139 and partially redundant amidases, AmiA/AmiB and AmiC [41,42]. Whereas AmiA and
140 AmiB are activated at the inner membrane/peptidoglycan interface by the
141 coordinated action of FtsE/FtsX and EnvC, activation of AmiC requires the OM-
142 anchored LytM domain-containing lipoprotein NlpD [43,44]. Under laboratory
143 conditions, the activity of only one of these two pathways is sufficient for septal
144 peptidoglycan splitting, whereas inhibition of both pathways leads to formation of
145 chains of partially divided cells, *i.e.* cells that have begun to divide but are blocked
146 at the step of septal peptidoglycan splitting [44]. A recent report showed that *dolP* is
147 necessary to complete septal peptidoglycan splitting and to promote cell separation
148 when the AmiA/AmiB pathway is inactive, somehow linking DolP to AmiC activation
149 [33]. Thus, the reduced fitness caused by silencing of *envC, ftsE or ftsX* in Δ*dolP* cells
150 (Fig. 1C) may be explained by impaired cell separation when both the AmiA/AmiB
151 and the AmiC pathways are not active. In keeping with this notion, *amiA* itself was
152 found among the negative fitness hits of the CRISPRi screen (Fig. 1C). *amiB* was
153 not a hit (Table S2), probably because AmiA is sufficient to split septal
154 peptidoglycan in the absence of other amidases [45].

155 Most importantly, the CRISPRi approach identified novel *dolP*-genetic
156 interactions that had a score similar to that obtained for *amiA* (Fig. 1C). These
157 included an interaction with *rseA*, encoding the inner membrane σ^E-sequestering
158 factor, as well as with *bamD*, encoding an essential subunit of the BAM complex
159 [34,46]. In accordance with the screen output, a serial dilution assay confirmed that
160 silencing of *bamD* (as well as *bamE*, encoding a stoichiometric interactor of BamD)
161 causes a fitness defect in cells lacking DolP (Fig. 1D, panels 8 and 9). In addition,
162 the interaction of *dolP* with *rseA* was confirmed in the genetic background of a

163 BW25113 strain (Fig. 1E). Further genes, involved in OMP biogenesis and more
164 generally in protein secretion, had a lower interaction score (Table S2 and Fig. S2C)
165 and are highlighted in Fig. 1C. These comprise *bamA*, the OMP chaperone-
166 encoding gene *surA*, as well as the genes encoding the Sec ancillary complex
167 SecDF-YajC that contributes to efficient secretion of proteins including OMPs [22] and
168 that was shown to interact with the BAM complex [47,48]. Collectively, the results of
169 the CRISPRi screen indicate that the function of DolP is particularly critical for cell
170 fitness upon inactivation of septal peptidoglycan hydrolysis by AmiA, as well as
171 when the assembly of proteins in the OM is impaired.

172

173 **DolP improves cell fitness when the OM undergoes stress**

174 At a first glance, the newly identified genetic interaction between *dolP* and
175 *bamD* (Figs. 1C and 1D) points to a possible role of DolP in OMP biogenesis.
176 However, the overall protein profile of the crude envelope fraction was not affected
177 by the deletion of *dolP* (Fig. S3A, lanes 1-4). OMPs, such as the very abundant
178 OmpA and OmpC [49], can be recognized by their characteristic heat-modifiable
179 migration patterns when separated by SDS-PAGE [50] (Fig. S3 A-D). The levels of
180 OmpA (Fig. S3B), LamB (Fig. S3C) and OmpC (Fig. S3D) were not affected in
181 Δ*dolP* samples. Similarly, the assembly kinetics of an autotransporter OMP was not
182 impaired (Fig. S3E). Importantly, the levels of proteins encoded by σ^E-upregulated
183 genes, such as BamA and BamE, were not increased in Δ*dolP* cells (Fig. 2A),
184 indicating a wild-type-like σ^E activity in this strain. The envelope protein profiles
185 were not affected also when *dolP* was deleted in cells lacking one of the OMP
186 periplasmic chaperones Skp or DegP (Fig. S3A, lanes 5-12), suggesting that DolP
187 does not play a function redundant with that of these periplasmic factors. Taken
188 together, these observations suggest that DolP is not crucial for efficient OMP
189 biogenesis. The genetic interaction of *dolP* with *bamD* and *surA* (Fig. 1C) may also
190 suggest that DolP is required for optimal survival when the OM undergoes

191 modifications caused by activation of the σ^E response [34,46,51]. This hypothesis is
192 supported by the observation that σ^E activation caused by *rseA* silencing or deletion
193 worsens the fitness of Δ*dolP* cells (Figs. 1C and 1E).

194 To further test the importance of DolP under envelope stress conditions, we
195 deleted *dolP* in a strain lacking *bamB,* which was identified with a lower genetic
196 score by the CRISPRi approach (Table S2). In Δ*bamB* cells, the σ^E response is
197 partially activated [19,52], causing the upregulation of *bam* genes (Fig. 2B). A strain
198 carrying the simultaneous deletion of *dolP* and *bamB* was viable but growth-
199 defective. Normal growth was restored by ectopic expression of a C-terminally
200 polyhistidine tagged DolP protein variant (Fig. 2C). The Δ*bamB* envelope protein
201 profile presented a marked reduction of the major heat-modifiable OMPs, OmpA
202 and OmpC, however the concomitant lack of DolP did not enhance this OMP defect
203 (Fig. S3A, lanes 13-18). Notably, phase-contrast analysis of the same Δ*dolP* Δ*bamB*
204 strain revealed a number of cells with altered morphology (Fig. 2D). This result
205 suggests that the reduced fitness of Δ*dolP* Δ*bamB* cells cannot be ascribed to an
206 exacerbation of the OMP biogenesis defect already caused by lack of BamB,
207 pointing to a different role of DolP under envelope stress conditions.

208

209 **DolP promotes growth in cells with increased levels of BAM complex.**

210 The σ^E response leads to alteration of the OM protein content, with an
211 increase of the level of the BAM complex and a reduction of numerous other
212 proteins, including the most abundant OMPs and some lipoproteins [25,53,54]. To gain
213 further insights into the role of DolP during activation of the σ^E response, we
214 explored the effect of prolonged overproduction of BAM. To this end, the genes
215 encoding wild-type BamABCD and a C-terminally polyhistidine-tagged BamE
216 protein variant were ectopically expressed via the isopropylthiogalactoside (IPTG)-
217 inducible *trc* promoter (P_{trc}) as a transcriptional unit, adapting a previously
218 established method [55]. With 400 μM IPTG, the concentration of BAM complex that

219 accumulated in the membrane fraction was roughly similar to the concentration of
220 the major OMPs OmpA or OmpC (Fig. 3A, lane 2). Importantly, we noticed that
221 prolonged BAM overproduction caused a partial detrimental effect in the wild-type
222 BW25113 strain (Fig. 3B). The excess of BamA was responsible for impaired
223 growth, as the excess of different subsets of BAM subunits that did not include
224 BamA or an excess of OmpA obtained using a similar overproduction plasmid (see
225 also the subsequent description of Fig. S7B) had no detectable effects in our growth
226 tests (Fig. 3B). The detrimental effect of BAM overproduction was caused by the
227 overaccumulation of BamA in the OM, as the overproduction of an assembly-
228 defective BamA variant, $BamA^{\Delta P1}$, that lacks the N-terminal POTRA1 motif and
229 largely accumulates in the periplasm [20], did not impair growth to the same extent
230 (Figs. S4A-C). Even a slight increment of BAM, due to the leaky transcriptional
231 activity of the *trc* promoter (Fig. 3A, lane 1) caused a mild but noticeable
232 deterioration of the OM permeability barrier to vancomycin (Fig. 3C), suggesting
233 that a small increment in BAM levels can enhance the permeability of the OM.
234 Strikingly, in the absence of vancomycin, we noticed that the detrimental effect
235 caused by IPTG-induced OM overaccumulation of BAM was more severe in a
236 Δ*dolP* strain (Fig. 3D). This difference was particularly evident with 200 μM IPTG,
237 which had only a minor inhibitory effect on the growth of wild-type cells but strongly
238 impaired the growth of a Δ*dolP* strain. Similar to *dolP*, *skp* is upregulated by σ^E and
239 its deletion causes sensitivity to vancomycin (Fig. S1B). In contrast to Δ*dolP*, a Δ*skp*
240 strain harbouring the same BAM overproduction plasmid could grow as the wild-
241 type reference (Fig. 3D), suggesting a specific effect of DolP in supporting growth
242 when BAM is overproduced.

243

244 **DolP interacts with BamA assembled in the OM**

245 The observed interaction between *dolP* and *bam* genes prompted us to
246 investigate whether DolP physically interacts with the BAM complex. To this end, a

247 construct encoding C-terminally protein A-tagged DolP was ectopically expressed in
248 Δ*dolP* cells. The envelope of cells expressing $DolP^{ProtA}$ was solubilized using
249 digitonin as main mild-detergent component prior to IgG-affinity chromatography
250 (Fig. 4A, coomassie staining). Site-specific enzymatic cleavage of an amino acid
251 linker between DolP and the protein A tag was used for protein elution. Notably,
252 BamA, BamC, BamD and BamE were immunodetected in the elution fraction of
253 protein A-tagged DolP (Fig. 4A, lane 3). In contrast, the inner membrane protein
254 CyoA and cytosolic RpoB were not detected. Next, BAM^{ProtA} (consisting of wild-type
255 BamABCD and a C-terminally protein A-tagged BamE protein variant) was
256 ectopically overproduced to isolate the BAM complex via IgG-affinity purification
257 (Fig. 4B, Coomassie staining). Importantly, in addition to the BamE bait and other
258 subunits of the BAM complex, DolP was also immunodetected in the elution fraction
259 (Fig. 4B, lane 3). Other proteins of the bacterial envelope (Skp, OmpA, and $F_1\beta$ of
260 the F_1F_O ATP synthase) or cytosolic RpoB were not detected (Fig. 4B). Taken
261 together, our native pull-down analysis indicates that DolP and BAM have affinity for
262 each other.

263 To explore whether the central BAM subunit, BamA, is a critical determinant
264 of the BAM-DolP interaction, we performed Ni-affinity purification using the
265 solubilized envelope fraction obtained from cells overproducing BamA and C-
266 terminally polyhistidine-tagged DolP. Under these conditions, BamA was efficiently
267 co-eluted together with $DolP^{His}$, demonstrating that BamA and DolP can interact
268 even in the absence of stoichiometric amounts of the BAM lipoproteins (Fig. 4C,
269 coomassie staining). To assess if the interaction of DolP and BAM takes place at
270 the OM, $DolP^{His}$ was overproduced together with the assembly-defective form
271 $BamA^{\Delta P1}$. When expressed together with $DolP^{His}$, assembly-defective $BamA^{\Delta P1}$ was
272 highly depleted in the corresponding eluate (Fig. 4C, lane 7), even though $BamA^{\Delta P1}$
273 was only marginally reduced in the crude envelope fraction with respect to wild-type
274 BamA (Fig. 4C, lane 3). In contrast to $BamA^{\Delta P1}$, the $BamA^{\Delta P2}$ variant, which is

275 efficiently assembled into the OM (Fig. S4), was co-eluted to a similar extent as
276 wild-type BamA (Fig. 4C, lane 8). This result indicates that DolP has affinity for OM-
277 assembled BamA.

278 In seeking a detergent that would interfere with the interaction of BAM and
279 DolP, and allow their purification as separate components, we solubilized the
280 envelope fraction with increasing amounts of n-dodecyl β-D-maltoside (DDM), a
281 detergent previously used to isolate the native BAM complex [55]. At concentrations of
282 DDM between 0.3% (w/v) and 1% (w/v), we observed a drastic reduction in the
283 amounts of BAM subunits that were co-eluted with $DolP^{His}$ (Fig. 4D), indicating that
284 the BAM-DolP interaction is sensitive to DDM. We thus used 1% (w/v) DDM to
285 extract and purify His-tagged DolP or His-tagged BAM as separate components
286 (Fig. 4E). When analyzed by blue native-PAGE and immunoblotting, purified DolP
287 gave rise to a diffused signal at around 450 kDa (Fig. 4F, lane 1), suggesting a
288 dynamic multimeric organization of this protein. Purified BAM migrated as expected
289 at 250 kDa (Fig. 4F, lane 7). When roughly equimolar amounts of purified BAM and
290 DolP were pre-incubated in the presence of a low DDM concentration and
291 subsequently resolved by blue native-PAGE, a complex with an apparent molecular
292 weight higher than that of the BAM complex was detected with both anti-BamA and
293 anti-DolP specific antibodies (Fig. 4F, lanes 3 to 6). Taken together our results
294 demonstrate that the BAM complex and DolP interact to form a larger complex and
295 that OM-assembled BamA is a critical determinant of this interaction. Only a portion
296 of BAM and DolP associate to form the BAM-DolP complex, indicating that the
297 interaction is substoichiometric.

298

299 **BamA overaccumulation in the OM reduces DolP mid-cell localization**

300 In light of our observation that DolP interacts with BAM, we asked whether
301 the envelope localization patterns of DolP and BAM are reciprocally linked. First, we
302 monitored the effect of DolP expression on the localization of the chromosomally

303 encoded BamD^{mCherry} subunit of the BAM complex. This protein generated a
304 fluorescence signal throughout the envelope that was not affected by the lack or the
305 overproduction of DolP (Fig. S5). Next, we checked the effect of BAM
306 overaccumulation in the OM on DolP localization. DolP associates with the OM and
307 accumulates at mid-cell during a late step of cell division [33]. To monitor the
308 localization of DolP, we used a strain harbouring a chromosomal *dolP-gfp* fusion
309 (Fig. 1A). The localization of the DolP^{GFP} fusion protein (Fig. S6A) was analyzed
310 concomitantly with other two chromosomally-encoded markers of the division
311 septum, ZipA^{mCherry} or NlpD^{mCherry}. ZipA is involved in an early step of divisome
312 assembly and accumulates at division sites before, as well as, during envelope
313 constriction (Fig. S6B) [56]. Instead, NlpD is a late marker of cell division involved in
314 the activation of AmiC and accumulates at septa that are already undergoing
315 constriction (Fig. S6C) [42,44]. DolP^{GFP} accumulated at mid-cell sites where the
316 envelope appeared invaginated, showing a localization pattern similar to that of
317 NlpD^{mCherry} (Fig. S6C) [33]. We investigated the effect of short-lived (1 hour) BAM
318 overproduction on DolP^{GFP} localization. Strikingly, we found that BAM
319 overproduction depleted DolP^{GFP} from mid-cell sites (Figs. 5A, center, and S8C). In
320 contrast, no obvious effects on cell division nor on mid-cell recruitment of ZipA^{mCherry}
321 and NlpD^{mCherry} was observed (Fig. S7A). The overproduction of BamA alone was
322 sufficient to alter the distribution of the DolP^{GFP} fluorescence signal in constricting
323 cells, reducing its intensity at constriction sites and enhancing it at decentred
324 positions along the cell axis (Fig. 5B, right plot). In contrast, the overproduction of
325 only the four BAM lipoproteins (Fig. 5A, right) as well as the overproduction of
326 OmpA (Fig. S7B) had no obvious effects on DolP mid-cell localization.

327 As BAM catalyzes OMP assembly, we asked whether this activity interferes
328 with DolP mid-cell localization. To address this question, we made use of an
329 inactive BamA mutant form (Fig. S8A) harbouring a polyhistidine peptide extension
330 at its C-terminal β-strand [57]. Similar to the overaccumulation of the BAM complex or

331 BamA, the overaccumulation of BamA^{His} interfered with DolP mid-cell localization
332 (Figs. S8B and S8C), without affecting ZipA^{mCherry} and NlpD^{mCherry} (Fig. S7C),
333 indicating that the cellular localization of DolP does not depend on the OMP-
334 assembly activity of BamA. In contrast, the ability of BamA to assemble into the OM
335 was a critical determinant of the observed septal depletion of DolP. In fact, the
336 periplasm-accumulating BamA$^{\Delta P1/His}$ variant (Fig. S8D) did not impair DolP^{GFP} mid-
337 cell localization (Fig. S8B, center), whereas the OM-overaccumulating BamA$^{\Delta P2/His}$
338 did (Figs. S8B, right, S8C, and S8D). Taken together, these results suggest that the
339 overaccumulation of BamA in the OM interferes with the recruitment of DolP at mid-
340 cell sites.

341

342 **DolP mid-cell localization is impaired under envelope stress conditions**

343 As DolP is critical for fitness under envelope stress conditions, we asked
344 whether the localization of DolP^{GFP} would be affected in mutants undergoing
345 envelope stress. To this end, we analyzed the localization of DolP^{GFP} in strains
346 lacking either the OMP chaperone SurA or the lipoprotein BamB. Both Δ*surA* and
347 Δ*bamB* strains are defective in OMP biogenesis and produce higher levels of BAM
348 complex due to activation of the σ^E response [19,51,52,58]. Importantly, the frequency of
349 mid-cell labelling by DolP^{GFP} was reduced in Δ*surA* cells both in minimal (Fig. S9A)
350 and LB (Fig. 5C) culture media. In contrast, lack of SurA did not affect septal
351 recruitment of the late cell division marker NlpD (Fig. S9B). The analysis of the
352 fluorescence plot profiles of constricted cells clearly showed a marked reduction of
353 the DolP^{GFP} signal at mid-cell sites and higher fluorescence levels in decentred
354 positions along the cell axis (Fig. 5C, right plot). As for the Δ*surA* strain, DolP^{GFP}
355 accumulated at the mid-cell with a lower frequency when *bamB* was deleted (Fig.
356 S9C). Together, these results indicate that the depletion of DolP at mid-cell sites
357 occurs during envelope stress-induced activation of the σ^E response.

358

359 **Discussion**

360 Despite its critical role in maintaining OM integrity, the reason why DolP is
361 upregulated by σ^E has remained unclear [32-34]. Here we demonstrate that DolP
362 interacts with the BAM complex and is crucial for fitness in cells with elevated σ^E
363 activity and when BAM overaccumulates in the OM. Our results have important
364 implications for the understanding of the mechanisms that coordinate OM and
365 peptidoglycan remodelling and help preserving envelope integrity.

366 A previous study [34] has shown that the concomitant deletion of *dolP* and *surA*
367 generates a severe synthetic growth defect. However, the role of DolP during
368 envelope stress and in OMP biogenesis had remained unclear [34,36]. Here we
369 demonstrate that DolP interacts with the BamA subunits of the BAM complex. DolP,
370 however, is not a stoichiometric component of the BAM complex and thus this
371 interaction is probably transient or has a lower affinity compared to the interactions
372 between BamA and the lipoproteins of the BAM complex. Several pieces of
373 evidence presented in this study suggest that DolP is not strictly required for OMP
374 assembly into the OM. In addition, we show that the deletion of *dolP* does not cause
375 envelope stress and activation of the σ^E response. Increased σ^E activity has been
376 reported to alleviate growth defects caused by the absence or inactivation of OMP
377 biogenesis factors [59-62]. On the contrary, activation of σ^E caused a growth defect in
378 a Δ*dolP* strain. This result suggests that, under envelope stress conditions, DolP
379 plays a fitness role that is not directly related to OMP biogenesis. More specifically,
380 we have obtained evidence that DolP opposes a detrimental effect that can derive
381 from the overaccumulation of BAM complex in the OM.

382 Further studies are warranted to determine the molecular bases of how DolP
383 promotes fitness during activation of the σ^E response. It is worth noting, however,
384 that DolP consists of two BON (bacterial OsmY and nodulation) domains, folding
385 motifs that have been proposed to interact with hydrophobic ligands such as lipids
386 [63]. Phospholipid-binding by DolP has been reported in a recent study [64]. A key

387 aspect of our results hints at a possible role of the lipid-binding function of DolP in
388 improving the fitness of cells that undergo envelope stress. We have shown that
389 DolP interacts with OM-assembled BamA, a subunit of the BAM complex that is
390 predicted to interfere with the organization of the surrounding lipid bilayer and to
391 generate an energetically favourable environment for the insertion of nascent OMPs
392 in the OM [65,66]. BamA-mediated membrane destabilization was shown by molecular
393 dynamics simulations, as well as by reconstituting BamA into proteoliposomes [9,67].
394 Here, we have provided evidence that the progressive overaccumulation of BAM in
395 the OM has an increasingly detrimental effect, enhancing the OM permeability at
396 low increments and impairing growth at higher levels. Our observation that DolP is
397 needed for optimal growth when the BAM complex overaccumulates in the OM is
398 compatible with a role of DolP in membrane stabilization at BAM sites. It remains to
399 be seen how DolP docks to BamA and whether it influences the organization of
400 BAM sites and of the surrounding lipid bilayer.

401 Another key finding of our study is that DolP septal localization is sensitive to
402 envelope stress conditions. During envelope stress, the OM undergoes a significant
403 alteration of its protein composition. Activation of the σ^E response triggers activation
404 of genes encoding OMP biogenesis factors, but also the posttranscriptional
405 downregulation of many OMPs including porins and OmpA [25]. OMPs are largely
406 arranged in clusters [68-70] embedded by highly organized LPS molecules in the
407 external leaflet of the OM [4] and the rigidity of their β-barrel structures contributes to
408 the mechanical stiffness of the OM [71]. Posttranscriptional downregulation targets of
409 σ^E activation also include the lipoproteins Pal and Lpp [53,54], which are critical for OM
410 integrity [72,73]. Whereas we have shown that BAM overaccumulation in the OM
411 influences DolP localization, it is possible that other modifications of the OM during
412 envelope stress contribute to impair the recruitment of DolP at constriction sites.

413 Distinct biogenesis and surveillance pathways are required to maintain the
414 protective function of the multi-layered envelope of Gram-negative bacteria [2]. Our

415 CRISPRi analysis shows that DolP promotes efficient cell growth when the AmiA
416 pathway of septal peptidoglycan splitting is impaired. This result is in line with the
417 conclusions of a previous study implicating DolP in the regulation of NlpD-mediated
418 activation of AmiC [33]. Cells lacking both NlpD and AmiC have reduced OM integrity
419 [33], which may contribute to explain the vancomycin sensitivity of Δ*dolP* cells. It
420 remains poorly understood whether envelope stress caused by the accumulation of
421 unfolded OMPs influences peptidoglycan remodelling. Intriguingly, our observation
422 that mid-cell localization of DolP is reduced in *surA* and *bamB* deletion strains
423 points to a possible role of DolP in linking envelope stress to septal peptidoglycan
424 hydrolysis. Reduced levels of DolP at mid-cell sites, and thus impaired AmiC
425 activation [33], could play an important role in coping with envelope stress, for
426 instance by regulating the window of time available to restore normal OMP
427 biogenesis prior to completing the formation of the new poles in the cell offspring.

428 Taken together, our results reveal an unprecedented link between activation
429 of the envelope stress response and a late step of cell division. The fitness role of
430 DolP during envelope stress emerges as an exploitable target in the development of
431 new antibacterial therapies.
432

433 **Materials and Methods**

434 **Bacterial strains and growth conditions**

435 All *E. coli* strains used in this study are listed in Table S3. Strains newly
436 generated for this study derive from BW25113 [Δ(*araD-araB*)*567* Δ(*rhaD-rhaB*)*568*
437 Δ*lacZ4787* (::rrnB-3) *hsdR514 rph-1*] [74] or MG1655 (F^- λ^- *ilvG*$^-$ *rfb-50 rph-1*) [75].
438 Deletions of *dolP*, *rseA, surA, bamB, degP, or skp* in a BW25113 strain were
439 achieved by P1 transduction of the Δ*dolP::kan*^{R}, Δ*rseA::kan*^{R}, Δ*surA::kan*^{R},
440 Δ*bamB::kan*^{R}, Δ*degP::kan*^{R} or Δ*skp::kan*^{R} alleles, respectively, obtained from the
441 corresponding Keio collection strains [37]. BW25113 derivative strains harbouring
442 chromosomal fusions of constructs encoding superfolder GFP downstream of *dolP*
443 or mCherry downstream of *nlpD*, *zipA* and *bamD* were obtained by λ-red
444 recombination as previously described [76]. Briefly, a kanamycin-resistance cassette
445 was amplified from plasmid pKD4 using oligonucleotides carrying extensions of
446 approximately 50 nucleotides homologous to regions immediately upstream or
447 downstream the stop codon of the interested genes. *Dpn*I-digested and purified
448 PCR products were electroporated into the BW25113 or derivative strains.
449 Recombinant clones were selected at 37°C on LB agar plates containing
450 kanamycin. When necessary, the *kan*^{R} cassette inserted into a mutated locus (gene
451 deletion or fusion) was removed upon transformation with the heat-curable plasmid
452 pCP20 [76]. The MG1655 derivative strain LC-E75, harbouring a dCas9-encoding
453 construct under the control of the P_{tet} promoter, has been described [38]. Cells were
454 cultured in home-made lysogeny broth (LB) medium (1% (w/v) tryptone, 0.5% (w/v)
455 yeast extract, 5 mg/ml (NaCl), commercially available Miller LB Broth (Sigma) or M9
456 minimal medium containing M9 salts (33.7 mM Na_2HPO_4, 22 mM KH_2PO_4, 8.55 mM
457 NaCl, 9.35 mM NH_4Cl) and supplemented with 0.2% w/v glycerol and all the amino
458 acids, or all amino acids except methionine and cysteine in the case of ^{35}S pulse-
459 chase labeling. Antibiotics were used at the following concentrations: ampicillin 100
460 μg/ml, kanamycin 50 μg/ml, vancomycin 60 μg/ml. For spot tests, cells were

461 cultured to mid-log phase, washed with M9 salts and serially diluted in ice-cold M9
462 salts prior to spotting on agar plates.

463

464 **Plasmid construction**

465 All plasmids used in data figures are listed in Table S4. Plasmids for the
466 ectopic expression of BAM subunits, DolP, or OmpA are derived from a pTrc99a
467 vector. The plasmid pBAM^{His} (pJH114), which harbours a P_{trc} promoter followed by
468 the *bamABCDE* open reading frames and an octahistidine tag fused downstream of
469 *bamE*, was described [55]. The region of pBAM^{His} comprising the segment that spans
470 from the *bamA* start codon to the *bamE* stop codon was deleted by site-directed
471 mutagenesis, generating pCtrl. Plasmids pBamA^{His} was generated by restriction-
472 free cloning, inserting the *bamA* ORF without its stop codon downstream of the P_{trc}
473 promoter and upstream of the octahistidine encoding region in pCtrl. pBamA^{His} was
474 subjected to site directed mutagenesis to generate pBamA, encoding wild-type,
475 non-tagged BamA. The *dolP* ORF amplified from the BW25113 genomic DNA was
476 used to replace the *bamABCDE* ORFs in pJH114 by restriction-free cloning,
477 generating pDolP^{His}. The plasmid pBamA-DolP^{His} was generated by restriction-free
478 cloning of the *bamA* ORF between the P_{trc} promoter and *dolP* in pDolP^{His}. Site-
479 directed mutagenesis was conducted on pBAM^{His} (pJH114) to obtain
480 pBamACDE^{His}, pBamABDE^{His}, pBamBCDE^{His}, pBamCDE^{His}. A sequence encoding
481 the tobacco etch virus protease cleavage site (TEV site) followed by a tandem
482 Protein-A tag was amplified from pYM10 [77] and fused by restriction-free cloning with
483 the last codon of the *bamE* gene in pBAM^{His} to generate pBAM^{ProtA}. A stop codon
484 was introduced downstream of the *bamE* last codon to generate pBAM. Plasmids
485 encoding the ΔP1 and ΔP2 BamA variant were obtained by site-directed
486 mutagenesis deleting the portion of *bamA* ORFs corresponding to residues E22-
487 K89 or P92-G172, respectively. The TEV site and the tandem Protein-A construct
488 amplified from pYM10 were inserted by restriction-free cloning downstream of the

489 *dolP* last codon in pDolP^{His}, generating pDolP^{ProtA}. pDolP was derived from
490 pDolP^{ProtA} using site-directed mutagenesis to introduce a stop codon immediately
491 downstream of the *dolP* ORF. The *ompA* ORF was amplified from the BW25113
492 genomic DNA and inserted by restriction-free cloning between P_{trc} and the His-tag
493 encoding construct of pCtrl to generate pOmpA^{His}. The sgRNAs plasmids are
494 derived from psgRNAcos [38]. To generate sgRNA-encoding plasmids the DNA
495 sequences AGCTGCACCTGCTGCGAATA (*bamD* sgRNA, plasmid pCAT187),
496 GTAAACCACTCGCTCCAGAG (*bamE* sgRNA, plasmid pCAT189),
497 CTCATCCGCGTGGGCGGAAA (*envC* sgRNA, plasmid pCAT191), and
498 CTGAGCCGCCGACCGATTTA (*ftsX* sgRNA, pCAT193) were inserted into a *Bsa*I
499 site of the psgRNAcos.

500

501 **CRISPRi screen and data analysis**

502 Strain LC-E75 (*dolP*$^{+}$) and its Δ*dolP* derivative were transformed with the
503 EcoWG1 library which contains 5 guides per gene as previously described [39]. After
504 culturing pooled transformant cells in LB at 37°C to early exponential phase (optical
505 density at 600 nm [OD_{600}] = 0.2), a sample was withdrawn for plasmid isolation
506 (t_{start}). Subsequently, cultures were supplemented with 1 μM anhydrotetracycline
507 (aTc) to induce dCas9 expression and further incubated at 37°C. When cultures
508 reached an OD_{600} of 2 they were diluted 1:100 into LB supplemented with 1 μM aTc
509 and incubated at the same temperature until an OD_{600} of 2. This step was repeated
510 one more time prior to withdrawing a sample for isolation of plasmid DNA (t_{end}).
511 Sequencing indexes were used to assign reads to each sample. Illumina
512 sequencing samples were prepared and analyzed as previously described [38].
513 Briefly, a two-step PCR was performed with Phusion polymerase (Thermo
514 Scientific) using indexed primers. The first PCR adds the first index and the second
515 PCR adds the second index and flow-cell attachment sequences. Pooled PCR
516 products were gel-purified. Sequencing was performed on a NextSeq550 machine

517 (Illumina). The total number of reads obtained for each sample was used to
518 normalize raw reads by sample size. Replicates were pooled to increase depth
519 before another normalization by sample size. Guides with less than 100 normalized
520 read counts in initial time points were discarded. For each screen, sgRNA fitness
521 was calculated as the log2-transformed ratio of normalized reads counts between
522 the final and the initial time point:

523 $$log2FC = log2\left(\frac{Normalized\ reads_{final} + 1}{Normalized\ reads_{initial} + 1}\right)$$

524 For each sample, log2FC values were centered by subtracting the median log2FC
525 of non-targeting control guides. We then calculated for each sgRNA the difference
526 of log2FC value between the Δ*dolP* screen and the *dolP*$^+$ screen. Guides were
527 ranked from the lowest negative values (negative fitness effect in Δ*dolP* compared
528 to *dolP*$^+$) to the highest positive values (positive fitness effect in Δ*dolP* compared to
529 *dolP*$^+$) and the significance of the interaction between *dolP* and each gene was
530 evaluated by performing a minimum hypergeometric (mHG) test on the ranked list
531 for each gene using the mHG R package (v. 1.1) [78]. False-discovery rate (FDR) was
532 used to correct p-values for multiple testing. For each gene, the median difference
533 of log2FC between Δ*dolP* and *dolP*$^+$ screens was used as a measure of the genetic
534 interaction.

535

536 **Cell fractionation**

537 To prepare whole-cell lysates, cells were cultured to early exponential phase
538 (OD_{600} = 0.2-0.3) in LB medium at 37°C and collected. Where indicated, IPTG was
539 added 60 min prior to cell collection. Cells were pelleted by centrifugation, washed
540 once with M9 salt and lysed with Laemmli Sample Buffer (BioRad) (69 mM Tris-HCl,
541 pH 6.8, 11.1% [v/v] glycerol, 1.1% [w/v] lithium dodecyl sulfate [LDS], 0.005% [w/v]
542 bromophenol blue, supplemented with 357 mM β-mercaptoethanol and 2 mM

543 phenylmethylsulfonyl fluoride [PMSF]). The total protein content was denatured at
544 98°C for 5 min prior SDS-PAGE analysis.

545 To perform lysozyme/EDTA lysis, cells were cultured to early exponential phase,
546 collected by centrifugation, resuspended in 33 mM Tris-HCl pH 8 to an OD_{600} of 1.
547 The cell suspension was then supplemented with 0.1 mg/ml lysozyme (Sigma), 2
548 mM EDTA and incubated on ice for 20 minutes to induce lysis. After addition of 10
549 mM $MgSO_4$, the membrane fraction was collected by centrifugation at 16000x *g*. The
550 supernatant was further centrifuged at 100000x *g* to remove any residual
551 membrane fraction, which was discarded. The obtained soluble fraction was
552 subjected to protein precipitation by adding 10% (w/v) trichloroacetic acid (TCA).
553 TCA precipitates were solubilized in Laemmli Sample Buffer (BioRad) prior to SDS-
554 PAGE analysis.

555 The crude envelope fractions directly analyzes by SDS-PAGE or used for
556 native affinity purification of affinity tagged BAM complex or DolP were prepared
557 from cells that were cultured in LB until early exponential phase and, where
558 indicated, supplemented with 400 μM IPTG for 1 hour to induce ectopic expression.
559 Cells were collected by centrifugation at 6000x *g* at 4°C, resuspended in 20 mM
560 Tris-HCl pH 8, and mechanically disrupted using a Cell Disruptor (Constant
561 Systems LTD) set to 0.82 kPa. The obtained cell lysate fractions were clarified by
562 centrifugation at 6000x *g* and 4°C. The supernatant was then subjected to
563 ultracentrifugation at 100000x *g* at 4°C to collect the envelope fraction.

564

565 **Isolation of native protein complexes by IgG- or nickel-affinity**
566 **chromatography**

567 The envelope fraction was resuspended at a concentration of approximately
568 10 mg/ml in solubilization buffer (20 mM Tris-HCl pH 7.4, 100 mM NaCl, 0.1 mM
569 EDTA, 2 mM PMSF) supplemented with EDTA-free protease inhibitor cocktail

570 (Roche), and 1.1% (w/v) of a mild detergent component corresponding to digitonin
571 (Merck) and n-dodecyl β-D-maltoside (DDM, Merck) as indicated in Figure Legends.
572 To facilitate extraction of membrane proteins, samples were subjected to mild
573 agitation for 1 hour at 4°C. Insoluble material was removed by centrifugation at
574 16000x *g* at 4°C. To perform IgG affinity purification, membrane-extracted proteins
575 were incubated for 1.5 hours at 4°C with purified human IgG (Sigma) that had been
576 previously coupled to CNBr-activated Sepharose beads (GE Healthcare). After
577 extensive washes of the resin with solubilization buffer containing 0.3% (w/v)
578 digitonin and 0.03% (w/v) DDM, bound proteins were eluted by incubation with
579 AcTEV protease (ThermoFisher) overnight at 4°C under mild agitation. To perform
580 nickel (Ni)-affinity purification, membrane-extracted proteins were supplemented
581 with 20 mM imidazole and incubated with Protino Ni-NTA agarose beads
582 (Macherey-Nagel) for 1 hour at 4°C. After extensive washes of the resin with
583 solubilization buffer supplemented with 50 mM imidazole, 0.3% (w/v) digitonin,
584 0.03% (w/v) DDM, and the EDTA-free protease inhibitor cocktail (Roche), bound
585 proteins were eluted using the same buffer supplemented with 500 mM imidazole.

586

587 ***In vitro* reconstitution of the BAM-DolP interaction and BN-PAGE analysis**

588 Envelope fractions were obtained from cells carrying pBAM^{His} or pDolP^{His}
589 and cultured until early exponential phase in LB medium at 37°C and subsequently
590 supplemented with 400 μM IPTG for 1.5 hours to induce the expression of the BAM
591 complex genes or *dolP*. The envelope fractions were solubilized and purified by Ni-
592 affinity and size exclusion chromatography, adapting a previously published
593 protocol. Briefly, after membrane solubilization with 50 mM Tris-HCl pH 8.0, 150
594 mM NaCl, and 1% (w/v) DDM, and removal of insoluble material by
595 ultracentrifugation at 100000x *g*, 4°C, soluble proteins were loaded onto a Ni-
596 column (HisTrap FF Crude, GE Healthcare) pre-equilibrated with 50 mM Tris-HCl
597 pH 8.0, 150 mM NaCl, and 0.03% (w/v) DDM (equilibration buffer), using an ÄKTA

598 Purifier 10 (GE Healthcare) at 4°C. The column containing bound proteins was
599 washed with equilibration buffer supplemented with 50 mM imidazole. Proteins were
600 eluted in equilibration buffer, applying a gradient of imidazole from 50 mM to 500
601 mM and further separated by gel filtration using an HiLoad 16/600 Superdex 200
602 (GE Healthcare) in equilibration buffer. Eluted proteins were concentrated using an
603 ultrafiltration membrane with a 10 kDa molecular weight cutoff (Vivaspin 6,
604 Sartorius). To reconstitute the BAM-DolP complex *in vitro,* equimolar concentrations
605 of purified BAM and DolP were used. Purified proteins were mixed in equilibration
606 buffer for 1 hour at 4°C or for 30 min at 25°C as indicated in Figure Legends. The
607 reaction was further diluted 1:4 times in ice-cold blue native buffer (20 mM Tris-HCl
608 pH 7.4, 50 mM NaCl, 0.1 mM EDTA, 1% [w/v] digitonin, 10% w/v glycerol) and ice
609 cold blue native loading buffer (5% coomassie brilliant blue G-250, 100 mM Bis-
610 Tris-HCl, pH 7.0, 500 mM 6-aminocaproic acid) prior to loading onto home-made 5-
611 13% blue native polyacrylamide gradient gels. Resolved protein complexes were
612 blotted onto a PVDF membrane and immunolabeled. Where non-relevant gel lanes
613 were removed, a white space was used to separate contiguous parts of the same
614 gel.

615

616 **Pulse-chase *in vivo* protein labeling**

617 Pulse-chase labeling of cellular proteins with radioactive ^{35}S methionine and
618 cysteine was conducted as previously described [79]. Briefly, overnight cultures were
619 washed and freshly diluted into M9 medium to OD_{600} = 0.03 and incubated at 37 °C.
620 When the cultures reached OD_{600} = 0.3, ectopic expression of EspP was induced by
621 adding 200 μM IPTG for 30 min. ^{35}S labelling was performed by supplementing
622 cultures with a mixture of [^{35}S]-methionine and [^{35}S]-cysteine followed after 30
623 seconds by the addition of an excess of cold methionine and cysteine. Samples
624 were withdrawn at different chase times, immediately mixed with an equal volume of
625 ice and subjected to TCA precipitation, prior to immunoprecipitation.

626

627 **Antibodies**

628 Proteins separated by SDS-PAGE or blue native-PAGE and blotted onto
629 PVDF membranes were immunodecorated using epitope-specific rabbit polyclonal
630 antisera with the following exceptions. The $F_1\beta$ subunit of the ATP F_1F_O synthase
631 was detected using a rabbit polyclonal antiserum raised against an epitope of the
632 homologous protein of *Saccharomyces cerevisiae* (Atp2). RpoB was detected using
633 a mouse monoclonal antibody (NeoClone Biotechnology). The secondary
634 immunodecoration was conducted using anti-rabbit or anti-mouse peroxidase-
635 conjugated antibodies produced in goat (Sigma). EspP immunoprecipitation was
636 conducted using a rabbit polyclonal antiserum specific for a C-terminal epitope of
637 EspP.

638

639 **Epifluorescence microscopy and analysis**

640 Overnight cultures of *E. coli* BW25113 and its derivative strains were diluted
641 into fresh M9 medium containing 0.2% glycerol or LB medium and grown at 30°C to
642 OD_{600} = 0.2-0.3. When indicated, cultures were supplemented with 400 μM of IPTG
643 to induce ectopic expression of plasmid-borne genes for 1 hour prior to collecting
644 samples for microscopy analysis. Culture volumes of 0.6 μl were deposited directly
645 onto slides coated with 1% (w/v) agarose in a phosphate-buffered saline solution
646 and visualized by epifluorescence microscopy. Cells were imaged at 30°C using an
647 Eclipse TI-E/B Nikon wide field epifluorescence inverted microscope with a phase
648 contrast objective (Plan APO LBDA 100X oil NA1.4 Phase) and a Semrock filter
649 mCherry (Ex: 562BP24; DM: 593; Em: 641BP75) or FITC (Ex: 482BP35; DM: 506;
650 Em: 536BP40). Images were acquired using a CDD OrcaR2 (Hamamatsu) camera
651 with illumination at 100% from a HG Intensilight source and with an exposure time
652 of 1-3 seconds, or using a Neo 5.5 sCMOS (Andor) camera with illumination at 60%

653 from a LED SPECTRA X source (Lumencor) with an exposure time of 2 seconds.
654 Nis-Elements AR software (Nikon) was used for image capture. Image analysis was
655 conducted using the Fiji and ImageJ software. The fraction of cells with DolP^{GPF}
656 signals at mid-cell sites was estimated using the Fiji Cell Counter plugin. Collective
657 profiles of fluorescence distribution versus the relative position along the cell axis
658 were generated using the Coli-Inspector macro run in ImageJ within the plugin
659 ObjectJ [80], selecting only cells with a constriction (80% of cell diameter) as qualified
660 objects.

661

662 **Acknowledgments**

663 We thank Harris Bernstein (NIDDK/NIH, Bethesda, MD) for providing key
664 reagents and for comments on the manuscript. We thank Tanneke Den Blaauwen
665 (University of Amsterdam) and Nathalie Dautin (IBPC/CNRS, Paris) for discussion.
666 We thank the Light Imaging Toulouse CBI (LITC) platform for assistance with and
667 maintenance of the microscopy instrumentation. Financial support was provided by:
668 the Fondation pour la Recherche Médicale to D.R.; the Chinese Scholarship
669 Council to Y.Y.; the Ecole Normale Supérieure to F.R.; the European Research
670 Council (Europe Union's Horizon 2020 research and innovation program, grant
671 agreement No 677823), the French governmental Investissement d'Avenir program
672 and the Laboratoire d'Excellence "Integrative Biology of Emerging Infectious
673 Diseases" (ANR-10-LABX-62-IBEID) to D.B.; the CNRS ATIP-Avenir program to
674 R.I.

675

676 **Author contribution**

677 R.I. conceived the project and wrote the manuscript; D.B. conceived and
678 developed the CRISPRi approach; R.I., D.B., D.R. L.C. and C.A. supervised the

experiments; D.R., Y.Y., L.O., F.R., L.C., V.M., C.M., G.M., A.C.-S, C.T., J.R. and C.A. performed the experiments and analyzed the data together with R.I. and D.B.; A.C.-S, D.R., Y.Y., L.O. and F.R. prepared the figures; all authors discussed the project and the experimental results, and commented on the manuscript.

684 **Figure Legends**

685

686 **Fig. 1. Genome-wide screen of *dolP* interactions.**

687 (**A**) The deletion of *dolP* impairs OM integrity. The indicated strains were serially
688 diluted and spotted onto LB agar plates lacking or supplemented with 60 μg/ml
689 vancomycin as indicated.

690 (**B**) Schematic representation of the CRISPR-based gene silencing approach. LC-
691 E75 (*dolP*$^+$) or its Δ*dolP* derivative strain, both carrying d*cas9* under the control of
692 an anhydrotetracycline (aTc)-inducible promoter in their chromosome were
693 transformed with a library of plasmids encoding gene-specific sgRNAs. The library
694 covers any *E. coli* MG1655 genetic features with an average of 5 sgRNAs per gene.
695 Pooled transformed cells were cultured to early exponential phase prior to plasmid
696 extraction and quantitative Illumina sequencing to assess the initial distribution of
697 sgRNA constructs in each culture (t_{start}). Upon addition of 1 μM aTc to induce
698 sgRNA-mediated targeting of d*cas9* for approximately 17 generations, samples of
699 cells from each culture were newly subjected to plasmid extraction and Illumina
700 sequencing to determine the final distribution of sgRNA constructs (t_{end}).

701 (**C**) Left: Comparison of gene scores obtained in *dolP*$^+$ and Δ*dolP* screens. The log2
702 fold-change (log2FC) between t_{end} and t_{start} calculated for each sgRNAs (Fig. S2B)
703 was grouped by gene target, and their median (Table S1) was used to derive fitness
704 gene scores. Right: Volcano plot of the *dolP* genetic interaction (GI) scores. The x-
705 axis shows a genetic interaction score calculated for each gene based on the
706 minimum hypergeometric (mHG) test conducted on the ranked difference of
707 sgRNA-specific log2FC values between the Δ*dolP* and the *dolP*$^+$ screens. The y-
708 axis shows the log10 of the false discovery rate (FDR) of the test. The dashed line
709 shows FDR = 0.05. In both panels, genes highlighted in orange have FDR < 0.05
710 and GI>1 whereas genes highlighted in red have FDR < 0.05 and GI>2.

711 (**D** and **E**) Validation of the genetic interactions determined in (C). (D) LC-E75
712 (*dolP*$^{+}$) or its Δ*dolP* derivative strain expressing sgRNAs that target the indicated
713 genes were serially diluted and spotted on LB agar lacking or supplemented with
714 aTc to induce expression of d*cas9*, as indicated. (E) BW25113 derivative cells
715 deleted of *rseA* or both *rseA* and *dolP* were transformed with an empty vector
716 (pCtrl) or a plasmid encoding DolP (pDolP^{His}). Ectopic expression of DolP^{His} was
717 driven by the leaky transcriptional activity of P_{trc} in the absence of IPTG. (D and E)
718 10-fold serial dilutions of the indicated transformants were spotted on LB agar.

719

720 **Fig. 2. DolP promotes fitness in cells that undergo envelope stress.**

721 (**A**) One and three folds of a sample containing the total cell lysate fraction from a
722 BW25113 (*dolP*$^{+}$) strain and a derivative Δ*dolP* strain were analyzed by SDS-PAGE
723 and immunoblotting using the indicated antisera.

724 (**B**) One, two and three folds of a sample containing the total cell lysate fraction from
725 a BW25113 (*bamB*$^{+}$) strain and a derivative Δ*bamB* strain were analyzed by SDS-
726 PAGE and immunoblotting using the indicated antisera.

727 (**C**) BW25113 and derivative cells deleted of *dolP, bamB* or both genes were
728 cultured, serially diluted and spotted on LB agar. A BW25113 derivative strain
729 deleted of both *dolP* and *bamB* and transformed with pDolP^{His} was cultured, serially
730 diluted and spotted on LB agar supplemented with ampicillin.

731 (**D**) Overnight cultures of BW25113 (control), Δ*dolP,* Δ*bamB and* Δ*dolP* Δ*bamB,*
732 were freshly diluted in LB medium and re-incubated at 30°C until OD_{600} = 0.3. Cell
733 were visualized on 1% (w/v) agarose pads by phase contrast microscopy. Bar = 5
734 μm.

735

736

737 **Fig. 3. DolP opposes an envelope detrimental effect caused by BAM**
738 **overaccumulation.**

739 (**A**) BW25113 cells harbouring pBAM^{His} as indicated were cultured and
740 supplemented with no IPTG or 400 μM IPTG for 1 hour prior to collecting cells. The
741 protein contents of the envelope fractions were analysed by SDS-PAGE and
742 coomassie staining. Prior to loading, samples were heated for 5 min at 90°C, a
743 temperature which is not sufficient to fully denature OmpA (folded OmpA, fOmpA).
744 The band of BamB overlaps with the band of the major porin unfolded OmpC
745 (uOmpC).

746 (**B**) BW25113 cells carrying a control empty vector (pCtrl), or the indicated plasmids
747 for ectopic overproduction of BAM or subsets of BAM subunits or OmpA were
748 serially diluted and spotted on LB agar containing 400 μM IPTG. The diagrams
749 show the overproduces proteins.

750 (**C**) Wild-type BW25113 cells carrying an empty control vector (pCtrl) or pBAM^{His}
751 were serially diluted and spotted on LB agar lacking or supplemented with 60 μg/ml
752 vancomycin. No IPTG was added to these medium.

753 (**D**) The BW25113 and the derivative Δ*dolP* or Δ*skp* strains carrying an empty
754 control vector (pCtrl) or pBAM^{His} were serially diluted and spotted on LB agar
755 supplemented with 400 or 200 μM IPTG, as indicated.

756

757 **Fig. 4. DolP associates with the BAM complex via an interaction with BamA.**

758 (**A**, **B**). The envelope fractions of BW25113 cells carrying the indicated plasmids
759 were solubilized with 1% (w/v) digitonin and 0.1% (w/v) DDM and subjected to IgG
760 affinity purification of either protein A-tagged DolP (A) or protein A-tagged BamE
761 (B). The load and elution fractions were analyzed by SDS-PAGE. The coomassie
762 staining of the elution of protein A-tagged DolP (A) or protein A-tagged BamE (B)
763 are shown below the diagrams representing overproduced proteins. Blotted protein

764 from load and elution fractions were detected by immunolabeling using the indicated
765 antisera. Load 0.5% (A) 1% (B); Elution 100%. The asterisk indicates the products
766 of TEV digestion obtained with samples containing $DolP^{ProtA}$ (A) or $BamE^{ProtA}$ (B).

767 (**C**) The envelope fractions of BW25113 cells carrying the plasmids overproducing
768 His-tagged DolP and the indicated BamA protein variants (deleted of POTRA1 or of
769 POTRA2) were solubilized with 1% (w/v) digitonin and 0.1% (w/v) DDM and
770 subjected to Ni-affinity purification. The load and elution fractions were analyzed by
771 SDS-PAGE. The coomassie staining of the elution of His-tagged DolP
772 overproduced together with wild-type BamA is shown below the diagram
773 representing overproduced proteins. Blotted protein from load and elution fractions
774 were detected by immunolabeling using the indicated antisera. Load 2%; Elution
775 100%.

776 (**D**) Equal aliquots of the envelope fraction of BW25113 cells expressing His-tagged
777 DolP were solubilized with the indicated concentrations (w/v) of digitonin and DDM:
778 1%, 0.1% (lane 1), 0.8%, 0.3% (lane 2), 0.3%, 0.8% (lane 3), 0.1%, 1% (lane 4).
779 His-tagged DolP was purified by Ni-affinity chromatography. In all cases, proteins
780 were eluted in the presence of 0.3% (w/v) digitonin and 0.03% (w/v) DDM. Load
781 0.2%; Elution 100%.

782 (**E**) The envelope fraction of BW25113 cells overproducing $DolP^{His}$ or the BAM
783 complex containing C-terminally His-tagged BamE was subjected to protein
784 extraction with 1% (w/v) DDM and Ni-affinity purification and gel filtration
785 chromatographies. The elution fractions were analyzed by SDS-PAGE and
786 coomassie staining. The double asterisk indicates a contaminant protein in the
787 elution of DolP.

788 (**F**) Roughly equimolar quantities of purified His-tagged BAM complex and DolP
789 were incubated alone for 1 hour at 4°C (lanes 1, 2 and 7), or together for 1 hour at
790 4°C (lanes 3 and 6) or for 30 min at 25°C (lanes 4 and 5), prior to blue native-PAGE
791 and immunoblotting using the indicated antisera.

792 **Fig. 5. BamA overaccumulation in the OM and envelope stress interfere with**
793 **mid-cell localization of DolP.**

794 (**A**) Overnight cultures of BW25113 cells harboring the chromosomal fusion *dolP-*
795 *gfp* and transformed with either pCtrl (empty vector) or pBAM^{His}, or pBamBCDE^{His}
796 were freshly diluted in minimal M9 medium, incubated at 30°C until OD_{600} = 0.1 and
797 supplemented with 400 μM IPTG for 1 hour. Cell samples were visualized on 1%
798 (w/v) agarose pads by phase contrast and fluorescence microscopy. Arrowheads
799 indicate envelope constriction sites between forming daughter cells. Bar = 5 μm.

800 (**B**) Left: Overnight cultures of BW25113 cells harboring the chromosomal fusion
801 *dolP-gfp* and transformed with either pCtrl (empty vector) or pBamA were cultured
802 and visualized as in (A). Bar = 5 μm. Right: The collective profiles of fluorescence
803 distribution versus the relative position along the cell axis were plotted for cells
804 transformed with pBamA (orange) and cells transformed with pCtrl (blue). Only cells
805 with a constriction (187, pBamA; 361, pCtrl) were taken into account for the
806 collective profile plots.

807 (**C**) Left: Overnight cultures of BW25113 (control) or Δ*surA* derivative cells carrying
808 the *dolP-gfp* chromosomal fusion were freshly diluted in LB medium and incubated
809 at 30°C until OD_{600} = 0.3. Cell samples were visualized as in (A). Bar = 5 μm. Right:
810 The collective profiles of fluorescence distribution versus the relative position along
811 the cell axis is shown for Δ*surA* cells (orange) and *surA*$^{+}$ control cells (blue). Only
812 cells with a constriction (320, Δ*surA*; 318, Control) were taken into account for the
813 collective profile plots.

814

815 **Fig. S1. The deletion of *dolP* severely impairs growth in the presence of**
816 **vancomycin.**

817 (**A**) BW25113 and Δ*dolP* cells were cultured in LB. The cell densities of both
818 cultures were monitored by measuring the OD_{600} at regular time intervals. The

819 graph reports mean values of independent cultures ± standard deviation (SD, *n* =
820 3).

821 (**B**) BW25113 (control) and the indicated deletion strains were cultured on LB agar
822 lacking or containing 60 μg/ml vancomycin.

823 (**C**) BW25113 and Δ*dolP* cells carrying the indicated plasmids were serially diluted
824 and spotted on LB lacking or containing 60 μg/ml vancomycin. Ectopic expression
825 was driven by the leaky transcriptional activity of P_{trc} in the absence of IPTG.

826

827 **Fig. S2. Reproducibility of the CRISPRi screens and ontology analysis of gene**
828 **hits.**

829 (**A**) The raw read counts of experimental replicates are very well correlated
830 (Pearson's r > 0.97) in both *dolP*$^+$ (left) and Δ*dolP* (right) screens.

831 (**B**) Log2FC values of each sgRNA are compared between the WT and Δ*dolP*
832 screens. Only guides targeting *envC*, *bamD*, and *rseA* are highlighted in orange, red
833 and cyan, respectively.

834 (**C**) Gene Ontology analysis of the genes with a significant synthetic interaction with
835 *dolP*. Using FDR<0.05 as a threshold, 27 genes were selected for Gene Ontology
836 (GO) analysis for cellular component (upper panel) or biological process (bottom
837 panel) [81]. Both analyses show an overrepresentation of genes associated with cell
838 envelope and membrane function.

839

840 **Fig. S3. DolP is not crucial for OMP biogenesis.**

841 (**A**) The protein contents of the indicated envelope fractions were analysed by SDS-
842 PAGE and coomassie staining. Prior to loading, samples were heated at 50°C
843 (boiling -) or 99°C (boiling +) for 10 min.

844 (**B**) The protein contents of the envelope fraction of BW25113 (*dolP*$^+$) or Δ*dolP* cells
845 were mixed with SDS-PAGE loading buffer, heated at 50°C (boiling -) or 99°C
846 (boiling +) for 10 min, and analyzed by SDS-PAGE and immunoblotting. Unfolded
847 (u) and folded (f) OmpA forms are indicated.

848 (**C** and **D**) The protein contents of the envelope fraction of BW25113 (*dolP*$^+$) and
849 Δ*dolP* cells was mixed with SDS-PAGE loading buffer, heated at the indicated
850 temperatures, separated by SDS-PAGE and immunoblotted using anti-LamB (C) or
851 anti-OmpC (D) antisera. LamB and OmpC form complexes (trimers), which are
852 resistant to SDS and require significant heating to be denatured. At progressively
853 higher temperatures, LamB (C) and OmpC (D) complexes are denatured and the
854 two proteins migrate as monomers (u, unfolded).

855 (**E**) The biogenesis of EspP, an autotransporter OMP of enterohemorrhagic *E. coli*
856 heterologously expressed in BW25113 cells, was monitored in time. The plasmid
857 pRI22 [79] harbouring the EspP encoding gene under the control of an IPTG-inducible
858 promoter was transformed into wild-type BW25113 (*dolP*$^+$) and Δ*dolP* cells. EspP is
859 a serine protease autotransporter of *Enterobacteriaceae*, and consists of an N-
860 terminal passenger domain secreted on the cell surface and a C-terminal domain
861 which is ultimately folded into an integral OM β-barrel structure [82]. EspP biogenesis
862 requires both periplasmic chaperones, such as SurA, and the BAM complex [79].
863 Once EspP assembly and secretion are completed, the passenger domain is
864 cleaved by an autocatalytic reaction that is catalyzed by residues of the folded β-
865 barrel domain facing the interior of the barrel. Thus, the proteolytic reaction can be
866 exploited to infer about completion of β-barrel folding and assembly [82]. To monitor
867 the kinetics of EspP autoproteolysis, cells carrying pRI22 were cultured in M9
868 minimal medium until early exponential phase, supplemented with 200 μM IPTG
869 and subjected to ^{35}S pulse-chase labelling. The total protein contents of samples
870 collected after the indicated chase times were subjected to immunoprecipitation
871 using an antiserum specific for an EspP C-terminal peptide. The asterisk indicates a

872 degradation product of EspP, likely generated by the OM protease OmpT, which
873 cleaves the N-terminal region of the passenger domain as it is secreted across the
874 OM[83]. A band corresponding to the EspP β-barrel domain is generated with a
875 similar time dependence in both *dolP*$^{+}$ and Δ*dolP* cells.

876

877 **Fig. S4. The detrimental effect of BAM overproduction is caused by the**
878 **overaccumulation of BAM in the OM**

879 (**A**) BW25113 cells were transformed with an empty vector or vectors for the ectopic
880 expression of the BAM complex containing protein A-tagged BamE (pBAM^{ProtA}), or
881 similar variants of the BAM complex including BamA$^{\Delta P1}$ (pBAM$^{\Delta P1/ProtA}$, lacking the
882 N-terminal POTRA1 motif) or BamA$^{\Delta P2}$ (pBAM$^{\Delta P2/ProtA}$, lacking the POTRA2 motif) in
883 place of wild-type BamA. In the presence of IPTG, overproduction of BAM$^{\Delta P1/ProtA}$
884 impaired growth to a lower extent compared to overproduction of BAM^{ProtA} or
885 BAM$^{\Delta P2/ProtA}$.

886 (**B**) The crude envelope fractions of cells overproducing BAM^{ProtA}, BAM$^{\Delta P1/ProtA}$, or
887 BAM$^{\Delta P2/ProtA}$ were solubilized with 1% (w/v) digitonin and 0.1% (w/v) DDM, and
888 subjected to native IgG-affinity chromatography. Elutions were analyzed by blue
889 native-PAGE and coomassie staining (lanes 1-3) or SDS-PAGE and immunoblotting
890 (lanes 4-6). Blue native-PAGE of the elution fraction containing wild-type BamA
891 resolved a coomassie stainable complex migrating with an apparent mass of 250
892 kDa, which corresponds to the BAM complex (lane 1). A roughly similar amount of
893 BAM complex was detected in the elution obtained with BamA$^{\Delta P2/ProtA}$ samples,
894 although in this case the BAM$^{\Delta P2}$ complex migrated slightly faster, accounting for
895 the BamA$^{\Delta P2}$ mass difference (lane 3). In contrast, the amount of BAM$^{\Delta P1/ProtA}$
896 variant was considerably lower (lane 2). The asterisk indicates that BamE is
897 obtained from TEV digestion of BamE^{ProtA}.

898 (**C**) Cells overproducing the indicated variants of the BAM complex were
899 fractionated. The membrane and soluble fractions, obtained upon treatment of
900 collected cells with lysozyme and EDTA were analyzed by SDS-PAGE and
901 immunoblotting. $BamA^{\Delta P1}$ was depleted from the total membrane fraction (lanes 1-
902 3), and accumulated in the soluble fraction containing the periplasmic protein DsbA
903 (lanes 4-6).

904

905 **Fig. S5. Effect of lack or overproduction of DolP on BAM localization.**

906 BW25113 derivative cells harbouring a *bamD-mCherry* chromosomal fusion were
907 visualized on 1% (w/v) agarose pads by fluorescence and phase-contrast
908 microscopy. Top: $dolP^+$ cells (control); Center: Δ*dolP* cells: Bottom: $dolP^+$ cells
909 carrying $pDolP^{His}$. Cells were cultured at 30°C in minimal M9 medium to OD_{600} =
910 0.5. IPTG (400 μM) was supplemented for 1 hour to induce ectopic expression of
911 $DolP^{His}$. Cells were visualized on 1% (w/v) agarose pads by fluorescence and
912 phase-contrast microscopy. Bar = 5 μm.

913

914 **Fig. S6. DolP accumulates at mid-cell sites during a late step of cell division.**

915 (**A**) The total protein content of cells harbouring the *dolP-gfp* chromosomal fusion
916 (lanes 1) or wild-type *dolP* (lanes 2) were analyzed by SDS-PAGE followed by
917 coomassie staining or immunoblotting using a DolP specific antiserum.

918 (**B, C**) BW25113-derivative cells harbouring the chromosomal fusion *dolP-gfp* and
919 either *zipA-mCherry* (B) or *nlpD-mCherry* (C) were cultured at 30°C in minimal M9
920 medium to OD_{600} = 0.2-0.3 and visualized on 1% (w/v) agarose pads by
921 fluorescence and phase-contrast microscopy. Bar = 5 μm.

922

923 **Fig. S7. Overproduction of BAM does not influence septal recruitment of NlpD**
924 **and ZipA.**

925 (**A**) BW25113-derivative cells harbouring the chromosomal fusion *dolP-gfp* and
926 *zipA-mCherry* or *nlpD-mCherry* were transformed with $pBAM^{His}$ (ectopic
927 overproduction of all BAM subunits, with His-tagged BamE). Cells were then
928 cultured at 30°C in minimal M9 medium supplemented with 400 μM IPTG for 1 hour
929 until OD_{600} = 0.2-0.3, and visualized on 1% (w/v) agarose pads by fluorescence
930 microscopy. The arrowheads indicate the localization of $DolP^{GFP}$, $ZipA^{mCherry}$ or
931 $NlpD^{mCherry}$ at division septa.

932 (**B**) Top: BW25113-derivative *dolP-gfp* cells transformed with pOmpA (ectopic
933 overproduction of His-tagged OmpA) were culture in LB medium and supplemented
934 with 400 μM IPTG or no IPTG for 1 hour prior to collecting cells. The total protein
935 content was analyzed by SDS-PAGE and immunoblotting using the indicated
936 antisera. Bottom: BW25113-derivative *dolP-gfp* cells transformed with $pOmpA^{His}$
937 were cultured in minimal M9 medium supplemented with 400 μM IPTG for 1 hour
938 until OD_{600} = 0.2-0.3, and visualized (A). Bar = 5 μm.

939 (**C**) BW25113-derivative cells harbouring the chromosomal fusion *dolP-gfp* and
940 *zipA-mCherry* or *nlpD-mCherry* were transformed with $pBamA^{His}$ (ectopic
941 overproduction of a partially inactive His-tagged form of BamA). Cells were then
942 cultured at 30°C in minimal M9 medium supplemented with 400 μM IPTG for 1 hour
943 until OD_{600} = 0.2-0.3, and visualized as in (A).

944

945 **Fig. S8. BamA overaccumulation in the OM impairs septal DolP localization.**

946 (**A**) The JCM166 BamA depletion strain or its transformants carrying plasmids
947 encoding $BamA^{His}$ or wild-type BamA and $DolP^{His}$ were cultured in the presence of
948 0.02% (w/v) arabinose (which induces transcription of a chromosomal copy of wild-
949 type *bamA* engineered downstream of an arabinose-inducible P_{bad} promoter). Serial

950 dilutions were spotted on LB agar devoid of or supplemented with 0.02% (w/v)
951 arabinose, as indicated. In the absence of arabinose, growth is supported by the
952 ectopic expression of wild-type BamA and not of its variant encoding C-terminally
953 His-tagged BamA.

954 (**B**) Overnight cultures of BW25113 cells harboring the chromosomal *dolP-gfp*
955 fusion and carrying the indicated plasmids were diluted in minimal M9 medium
956 supplemented with 400 μM IPTG. The cells were grown at 30°C to OD_{600} = 0.2-0.3
957 and visualized on 1% (w/v) agarose pads by fluorescence microscopy. The arrows
958 indicate envelope constriction sites between forming daughter cells. Bar = 5 μm.

959 (**C**) Counting of BW25113 cells presenting septal $DolP^{GFP}$ fluorescent signals. *dolP-*
960 *gfp* cells carring $pBAM^{His}$, $pBamA^{His}$, $pBamA^{\Delta P1/His}$ or $pBamA^{\Delta P2/His}$ (analyzed by
961 fluorescence microscopy and shown in Fig. 5A and in Fig. S8B) were counted. The
962 percentage of cells presenting fluorescent $DolP^{GFP}$ signals at the mid-cell in
963 samples overproducing all five BAM subunits or only one of the indicated BamA
964 variants was normalized to the same fraction obtained for cells carrying the control
965 empty vector (pCtrl). Bar charts display a mean value ± SD (n = 3). More than 300
966 cells were counted in each experiment.

967 (**D**) BW25113 cells carrying the indicated plasmids were cultured and supplemented
968 with 400 μM IPTG to induce ectopic expression of $BamA^{His}$ and its mutant forms.
969 Collected cells were subjected to lysozyme/EDTA lysis to obtain the total membrane
970 and soluble fractions. The protein contents of the indicated cell fractions were
971 separated by SDS-PAGE and immunolabeled with the indicated antisera.

972

973 **Fig. S9. Envelope stress influences DolP localization**

974 (**A**) Overnight cultures of BW25113 (Control) or Δ*surA* derivative cells carrying the
975 *dolP-gfp* chromosomal fusion were freshly diluted in M9 medium and incubated at
976 30°C till OD_{600} = 0.03 and visualized on 1% (w/v) agarose pads by contrast and

977 fluorescence microscopy. Bar = 5 μm. The arrows indicate envelope constriction
978 sites between forming daughter cells. The percentage of cells presenting
979 fluorescent DolP^{GFP} signals at division septa in Δ*surA* cells was normalized to the
980 same fraction obtained for the control cells and reported below the micrograph.
981 More than 1000 cells were counted in each sample.

982 (**B**) Overnight cultures of BW25113 (control) or Δ*surA* derivative cells carrying the
983 *dolP-gfp* and *nlpD-mCherry* chromosomal fusions were freshly diluted in LB medium
984 and incubated at 30°C until OD_{600} = 0.3 prior to visualization by contrast and
985 fluorescence microscopy. Bar = 5 μm. The arrows indicate envelope constriction
986 sites between forming daughter cells

987 (**C**) Overnight cultures of Δ*bamB* cells harboring the chromosomal *dolP-gfp* fusion
988 were diluted in minimal M9 medium, cultured at 30°C to OD_{600} = 0.3 and visualized
989 on 1% (w/v) agarose pads by contrast and fluorescence microscopy. The arrows
990 indicate envelope constriction sites between forming daughter cells. Bar = 5 μm.
991 The percentage of cells presenting fluorescent DolP^{GFP} signals at division septa in
992 Δ*bamB* cells was normalized to the same fraction obtained for the control cells
993 (BW25113 carrying the *dolP-gfp* chromosomal fusion) and reported below the
994 micrograph. More than 300 cells were counted.
995

996 **Table S1. Log2FC values of sgRNAs in the WT or Δ*dolP* screen.**

997 See source data file (Table S1)

998

999 **Table S2. Genetic interaction scores.**

1000 See source data file (Table S2)

1001

1002 **Table S3: List of strains**

1003

Name	Genotype and relevant features	Source
BW25113	Δ(*araD-araB*)*567* Δ(*rhaD-rhaB*)*568* Δ*lacZ4787*(::*rrnB-3*) *hsdR514 rph-1 (wild-type reference)*	Grenier *et al.*, 2014 [74]
Δ*rseA*	BW25113 *rseA::kan*	This study
Δ*dolP*	BW25113 *dolP::kan*	This study
Δ*bamB*	BW25113 *bamB::kan*	This study
Δ*bamB* Δ*dolP*	BW25113 Δ*bamB dolP::kan*	This study
Δ*dolP* Δ*rseA*	BW25113 Δ*dolP rseA::kan*	This study
Δ*skp*	BW25113 *skp::kan*	This study
Δ*dolP* Δ*skp*	BW25113 Δ*dolP skp::kan*	This study
Δ*degP*	BW25113 *degP::kan*	This study
Δ*dolP* Δ*degP*	BW25113 Δ*dolP degP::kan*	This study
dolP-gfp	BW25113 *dolP-gfp*	This study
Δ*surA*	BW25113 *surA::kan*	This study
Δ*surA dolP-gfp*	BW25113 *surA::kan dolP-gfp*	This study
Δ*bamB dolP-gfp*	BW25113 *bamB::kan dolP-gfp*	This study
Δ*dolP bamD-mCherry*	BW25113 Δ*dolP bamD-mCherry*	This study
bamD-mCherry	BW25113 *bamD-mCherry*	This study
dolP-gfp nlpD-mCherry	BW25113 *dolP-gfp nlpD-mCherry*	This study
Δ*surA dolP-gfp nlpD-mCherry*	BW25113 *dolP-gfp nlpD-mCherry surA::kan*	This study
dolP-gfp zipA-mCherry	BW25113 *dolP-gfp zipA-mCherry*	This study
JCM166	MC4100 *ara*$^{r/-}$ Δ(*λatt-lom*)::*bla* P_{BAD}*yaeT araC* Δ*yaeT* (BamA depletion strain)	Wu *et al.*, 2005 [19]
LC-E75	F^- λ^- *ilvG*$^-$ *rfb-50 rph-1 186attB*::P_{tet}-*dcas9*, λ*attB::mCherry*	Cui *et al.*, 2018 [38]
LC-E75 Δ*dolP*	LC-E75 *dolP::kan*	This study

1004

1005 **Table S4: List of plasmids**

1006

Name	Relevant features	Source
pCtrl	Reference empty vector for ectopic protein expression	This study
pBAM	Ectopic expression of all 5 BAM subunits	This study
$pBAM^{His}$ (pJH114)	Ectopic expression of all 5 BAM subunits; BamE is C-terminally His-tagged	Roman Hernandez *et al.*, 2014 [55]
$pBAM^{ProtA}$	Ectopic expression of all 5 BAM subunits; BamE is C-terminally Protein A-tagged; a TEV site amino acid linker is positioned immediately upstream of the tag	This study
$pBAM^{\Delta P1/ProtA}$	Ectopic expression of all 5 BAM subunits; BamA harbours the deletion of POTRA1 and BamE is C-terminally Protein A-tagged; a TEV site amino acid linker is positioned immediately upstream of the tag	This study
$pBAM^{\Delta P2/ProtA}$	Ectopic expression of all 5 BAM subunits; BamA harbours the deletion of POTRA2 and BamE is C-terminally Protein A-tagged; a TEV site amino acid linker is positioned immediately upstream of the tag	This study
$pBamABDE^{His}$	Ectopic expression of BamA, BamB, BamD and BamE subunits; BamE is C-terminally His-tagged	This study
$pBamACDE^{His}$	Ectopic expression of BamA, BamC, BamD and BamE subunits; BamE is C-terminally His-tagged	This study

pBamBCDE^{His}	Ectopic expression of BamB, BamC, BamD and BamE subunits; BamE is C-terminally His-tagged	This study
pBamCDE^{His}	Ectopic expression of BamC, BamD and BamE subunits; BamE is C-terminally His-tagged	This study
pBamA	Ectopic expression of wild-type BamA	This study
pBamA^{His}	Ectopic expression of C-terminally His-tagged BamA	This study
pBamA$^{\Delta P1/His}$	Ectopic expression of a C-terminally His-tagged BamA variant lacking POTRA1	This study
pBamA$^{\Delta P2/His}$	Ectopic expression of a C-terminally His-tagged BamA variant lacking POTRA2	This study
pBamA-DolP^{His}	Ectopic expression of BamA and C-terminally His-tagged DolP	This study
pBamA$^{\Delta P1}$-DolP^{His}	Ectopic expression of a BamA variant lacking POTRA1 and C-terminally His-tagged DolP	This study
pBamA$^{\Delta P2}$-DolP^{His}	Ectopic expression of a BamA variant lacking POTRA2 and C-terminally His-tagged DolP	This study
pDolP	Ectopic expression of wild-type DolP	This study
pDolP^{ProtA}	Ectopic expression of C-terminally protein A-tagged DolP; a TEV site amino acid linker is positioned immediately upstream of the tag	This study
pDolP^{His}	Ectopic expression of C-terminally His-tagged DolP	This study
pOmpA^{His}	Ectopic expression of C-terminally His-tagged OmpA	This study

pRI22	Ectopic expression of EspP	Ieva *et al.*, 2009 [79]
psgRNAcos	Reference empty vector for expression of sgRNAs	Cui *et al.*, 2018 [38]
psgRNA*bamD* (pCAT187)	Expression of a *bamD*-specific sgRNA	This study
psgRNA*bamE* (pCAT189)	Expression of a *bamE*-specific sgRNA	This study
psgRNA*envC* (pCAT191)	Expression of a *envC*-specific sgRNA	This study
psgRNA*ftsX* (pCAT193)	Expression of a *ftsX*-specific sgRNA	This study

1007

1008

1009 **References**

1010 1 den Blaauwen, T., Hamoen, L. W. & Levin, P. A. The divisome at 25: the
1011 road ahead. *Current opinion in microbiology* **36**, 85-94,
1012 doi:10.1016/j.mib.2017.01.007 (2017).
1013 2 Egan, A. J. F., Errington, J. & Vollmer, W. Regulation of peptidoglycan
1014 synthesis and remodelling. *Nature reviews. Microbiology*,
1015 doi:10.1038/s41579-020-0366-3 (2020).
1016 3 Calmettes, C., Judd, A. & Moraes, T. F. Structural Aspects of Bacterial Outer
1017 Membrane Protein Assembly. *Advances in experimental medicine and*
1018 *biology* **883**, 255-270, doi:10.1007/978-3-319-23603-2_14 (2015).
1019 4 Nikaido, H. Molecular basis of bacterial outer membrane permeability
1020 revisited. *Microbiology and molecular biology reviews : MMBR* **67**, 593-656,
1021 doi:10.1128/mmbr.67.4.593-656.2003 (2003).
1022 5 Ranava, D., Caumont-Sarcos, A., Albenne, C. & Ieva, R. Bacterial
1023 machineries for the assembly of membrane-embedded beta-barrel proteins.
1024 *FEMS microbiology letters* **365**, doi:10.1093/femsle/fny087 (2018).
1025 6 Schiffrin, B., Brockwell, D. J. & Radford, S. E. Outer membrane protein
1026 folding from an energy landscape perspective. *BMC biology* **15**, 123,
1027 doi:10.1186/s12915-017-0464-5 (2017).
1028 7 Webb, C. T., Heinz, E. & Lithgow, T. Evolution of the beta-barrel assembly
1029 machinery. *Trends in microbiology* **20**, 612-620,
1030 doi:10.1016/j.tim.2012.08.006 (2012).
1031 8 Voulhoux, R., Bos, M. P., Geurtsen, J., Mols, M. & Tommassen, J. Role of a
1032 highly conserved bacterial protein in outer membrane protein assembly.
1033 *Science (New York, N.Y.)* **299**, 262-265, doi:10.1126/science.1078973
1034 (2003).
1035 9 Noinaj, N., Kuszak, A. J., Gumbart, J. C., Lukacik, P., Chang, H., Easley, N.
1036 C., Lithgow, T. & Buchanan, S. K. Structural insight into the biogenesis of
1037 beta-barrel membrane proteins. *Nature* **501**, 385-390,
1038 doi:10.1038/nature12521 (2013).
1039 10 Iadanza, M. G., Higgins, A. J., Schiffrin, B., Calabrese, A. N., Brockwell, D.
1040 J., Ashcroft, A. E., Radford, S. E. & Ranson, N. A. Lateral opening in the
1041 intact beta-barrel assembly machinery captured by cryo-EM. *Nature*
1042 *communications* **7**, 12865, doi:10.1038/ncomms12865 (2016).
1043 11 Gu, Y., Li, H., Dong, H., Zeng, Y., Zhang, Z., Paterson, N. G., Stansfeld, P.
1044 J., Wang, Z., Zhang, Y., Wang, W. & Dong, C. Structural basis of outer
1045 membrane protein insertion by the BAM complex. *Nature* **531**, 64-69,
1046 doi:10.1038/nature17199 (2016).
1047 12 Bakelar, J., Buchanan, S. K. & Noinaj, N. The structure of the beta-barrel
1048 assembly machinery complex. *Science (New York, N.Y.)* **351**, 180-186,
1049 doi:10.1126/science.aad3460 (2016).
1050 13 Doerner, P. A. & Sousa, M. C. Extreme Dynamics in the BamA beta-Barrel
1051 Seam. *Biochemistry* **56**, 3142-3149, doi:10.1021/acs.biochem.7b00281
1052 (2017).
1053 14 Gessmann, D., Chung, Y. H., Danoff, E. J., Plummer, A. M., Sandlin, C. W.,
1054 Zaccai, N. R. & Fleming, K. G. Outer membrane beta-barrel protein folding is
1055 physically controlled by periplasmic lipid head groups and BamA.
1056 *Proceedings of the National Academy of Sciences of the United States of*
1057 *America* **111**, 5878-5883, doi:10.1073/pnas.1322473111 (2014).

15 Doyle, M. T. & Bernstein, H. D. Bacterial outer membrane proteins assemble via asymmetric interactions with the BamA beta-barrel. *Nature communications* **10**, 3358, doi:10.1038/s41467-019-11230-9 (2019).

16 Tomasek, D., Rawson, S., Lee, J., Wzorek, J. S., Harrison, S. C., Li, Z. & Kahne, D. Structure of a nascent membrane protein as it folds on the BAM complex. *Nature*, doi:10.1038/s41586-020-2370-1 (2020).

17 Sklar, J. G., Wu, T., Gronenberg, L. S., Malinverni, J. C., Kahne, D. & Silhavy, T. J. Lipoprotein SmpA is a component of the YaeT complex that assembles outer membrane proteins in Escherichia coli. *Proceedings of the National Academy of Sciences of the United States of America* **104**, 6400-6405, doi:10.1073/pnas.0701579104 (2007).

18 Kim, S., Malinverni, J. C., Sliz, P., Silhavy, T. J., Harrison, S. C. & Kahne, D. Structure and function of an essential component of the outer membrane protein assembly machine. *Science (New York, N.Y.)* **317**, 961-964, doi:10.1126/science.1143993 (2007).

19 Wu, T., Malinverni, J., Ruiz, N., Kim, S., Silhavy, T. J. & Kahne, D. Identification of a multicomponent complex required for outer membrane biogenesis in Escherichia coli. *Cell* **121**, 235-245, doi:10.1016/j.cell.2005.02.015 (2005).

20 Bennion, D., Charlson, E. S., Coon, E. & Misra, R. Dissection of beta-barrel outer membrane protein assembly pathways through characterizing BamA POTRA 1 mutants of Escherichia coli. *Molecular microbiology* **77**, 1153-1171, doi:10.1111/j.1365-2958.2010.07280.x (2010).

21 Rizzitello, A. E., Harper, J. R. & Silhavy, T. J. Genetic evidence for parallel pathways of chaperone activity in the periplasm of Escherichia coli. *Journal of bacteriology* **183**, 6794-6800, doi:10.1128/jb.183.23.6794-6800.2001 (2001).

22 Crane, J. M. & Randall, L. L. The Sec System: Protein Export in Escherichia coli. *EcoSal Plus* **7**, doi:10.1128/ecosalplus.ESP-0002-2017 (2017).

23 Walsh, N. P., Alba, B. M., Bose, B., Gross, C. A. & Sauer, R. T. OMP peptide signals initiate the envelope-stress response by activating DegS protease via relief of inhibition mediated by its PDZ domain. *Cell* **113**, 61-71, doi:10.1016/s0092-8674(03)00203-4 (2003).

24 Ades, S. E. Regulation by destruction: design of the sigmaE envelope stress response. *Current opinion in microbiology* **11**, 535-540, doi:10.1016/j.mib.2008.10.004 (2008).

25 Rhodius, V. A., Suh, W. C., Nonaka, G., West, J. & Gross, C. A. Conserved and variable functions of the sigmaE stress response in related genomes. *PLoS biology* **4**, e2, doi:10.1371/journal.pbio.0040002 (2006).

26 Guillier, M., Gottesman, S. & Storz, G. Modulating the outer membrane with small RNAs. *Genes & development* **20**, 2338-2348, doi:10.1101/gad.1457506 (2006).

27 De Las Penas, A., Connolly, L. & Gross, C. A. SigmaE is an essential sigma factor in Escherichia coli. *Journal of bacteriology* **179**, 6862-6864, doi:10.1128/jb.179.21.6862-6864.1997 (1997).

28 Missiakas, D., Mayer, M. P., Lemaire, M., Georgopoulos, C. & Raina, S. Modulation of the Escherichia coli sigmaE (RpoE) heat-shock transcription-factor activity by the RseA, RseB and RseC proteins. *Molecular microbiology* **24**, 355-371, doi:10.1046/j.1365-2958.1997.3601713.x (1997).

29 De Las Penas, A., Connolly, L. & Gross, C. A. The sigmaE-mediated response to extracytoplasmic stress in Escherichia coli is transduced by RseA and RseB, two negative regulators of sigmaE. *Molecular microbiology* **24**, 373-385, doi:10.1046/j.1365-2958.1997.3611718.x (1997).
30 Nicoloff, H., Gopalkrishnan, S. & Ades, S. E. Appropriate Regulation of the sigma(E)-Dependent Envelope Stress Response Is Necessary To Maintain Cell Envelope Integrity and Stationary-Phase Survival in Escherichia coli. *Journal of bacteriology* **199**, doi:10.1128/jb.00089-17 (2017).
31 Mitchell, A. M. & Silhavy, T. J. Envelope stress responses: balancing damage repair and toxicity. *Nature reviews. Microbiology* **17**, 417-428, doi:10.1038/s41579-019-0199-0 (2019).
32 Morris, F. C., Wells, T. J., Bryant, J. A., Schager, A. E., Sevastsyanovich, Y. R., Squire, D. J. P., Marshall, J., Isom, G. L., Rooke, J., Maderbocus, R., Knowles, T. J., Overduin, M., Rossiter, A. E., Cunningham, A. F. & Henderson, I. R. YraP Contributes to Cell Envelope Integrity and Virulence of Salmonella enterica Serovar Typhimurium. *Infection and immunity* **86**, doi:10.1128/iai.00829-17 (2018).
33 Tsang, M. J., Yakhnina, A. A. & Bernhardt, T. G. NlpD links cell wall remodeling and outer membrane invagination during cytokinesis in Escherichia coli. *PLoS genetics* **13**, e1006888, doi:10.1371/journal.pgen.1006888 (2017).
34 Onufryk, C., Crouch, M. L., Fang, F. C. & Gross, C. A. Characterization of six lipoproteins in the sigmaE regulon. *Journal of bacteriology* **187**, 4552-4561, doi:10.1128/jb.187.13.4552-4561.2005 (2005).
35 Seib, K. L., Haag, A. F., Oriente, F., Fantappie, L., Borghi, S., Semchenko, E. A., Schulz, B. L., Ferlicca, F., Taddei, A. R., Giuliani, M. M., Pizza, M. & Delany, I. The meningococcal vaccine antigen GNA2091 is an analogue of YraP and plays key roles in outer membrane stability and virulence. *FASEB journal : official publication of the Federation of American Societies for Experimental Biology* **33**, 12324-12335, doi:10.1096/fj.201900669R (2019).
36 Bos, M. P., Grijpstra, J., Tommassen-van Boxtel, R. & Tommassen, J. Involvement of Neisseria meningitidis lipoprotein GNA2091 in the assembly of a subset of outer membrane proteins. *The Journal of biological chemistry* **289**, 15602-15610, doi:10.1074/jbc.M113.539510 (2014).
37 Baba, T., Ara, T., Hasegawa, M., Takai, Y., Okumura, Y., Baba, M., Datsenko, K. A., Tomita, M., Wanner, B. L. & Mori, H. Construction of Escherichia coli K-12 in-frame, single-gene knockout mutants: the Keio collection. *Molecular systems biology* **2**, 2006.0008, doi:10.1038/msb4100050 (2006).
38 Cui, L., Vigouroux, A., Rousset, F., Varet, H., Khanna, V. & Bikard, D. A CRISPRi screen in E. coli reveals sequence-specific toxicity of dCas9. *Nature communications* **9**, 1912, doi:10.1038/s41467-018-04209-5 (2018).
39 Calvo-Villamanan, A., Ng, J. W., Planel, R., Menager, H., Chen, A., Cui, L. & Bikard, D. On-target activity predictions enable improved CRISPR-dCas9 screens in bacteria. *Nucleic acids research*, doi:10.1093/nar/gkaa294 (2020).
40 Pichoff, S., Du, S. & Lutkenhaus, J. Roles of FtsEX in cell division. *Research in microbiology* **170**, 374-380, doi:10.1016/j.resmic.2019.07.003 (2019).
41 Heidrich, C., Templin, M. F., Ursinus, A., Merdanovic, M., Berger, J., Schwarz, H., de Pedro, M. A. & Holtje, J. V. Involvement of N-acetylmuramyl-L-alanine amidases in cell separation and antibiotic-induced autolysis of

1157 Escherichia coli. *Molecular microbiology* **41**, 167-178, doi:10.1046/j.1365-
1158 2958.2001.02499.x (2001).
1159 42 Uehara, T., Dinh, T. & Bernhardt, T. G. LytM-domain factors are required for
1160 daughter cell separation and rapid ampicillin-induced lysis in Escherichia coli.
1161 *Journal of bacteriology* **191**, 5094-5107, doi:10.1128/jb.00505-09 (2009).
1162 43 Yang, D. C., Peters, N. T., Parzych, K. R., Uehara, T., Markovski, M. &
1163 Bernhardt, T. G. An ATP-binding cassette transporter-like complex governs
1164 cell-wall hydrolysis at the bacterial cytokinetic ring. *Proceedings of the*
1165 *National Academy of Sciences of the United States of America* **108**, E1052-
1166 1060, doi:10.1073/pnas.1107780108 (2011).
1167 44 Uehara, T., Parzych, K. R., Dinh, T. & Bernhardt, T. G. Daughter cell
1168 separation is controlled by cytokinetic ring-activated cell wall hydrolysis. *The*
1169 *EMBO journal* **29**, 1412-1422, doi:10.1038/emboj.2010.36 (2010).
1170 45 Chung, H. S., Yao, Z., Goehring, N. W., Kishony, R., Beckwith, J. & Kahne,
1171 D. Rapid beta-lactam-induced lysis requires successful assembly of the cell
1172 division machinery. *Proceedings of the National Academy of Sciences of the*
1173 *United States of America* **106**, 21872-21877, doi:10.1073/pnas.0911674106
1174 (2009).
1175 46 Malinverni, J. C., Werner, J., Kim, S., Sklar, J. G., Kahne, D., Misra, R. &
1176 Silhavy, T. J. YfiO stabilizes the YaeT complex and is essential for outer
1177 membrane protein assembly in Escherichia coli. *Molecular microbiology* **61**,
1178 151-164, doi:10.1111/j.1365-2958.2006.05211.x (2006).
1179 47 Carlson, M. L., Stacey, R. G., Young, J. W., Wason, I. S., Zhao, Z., Rattray,
1180 D. G., Scott, N., Kerr, C. H., Babu, M., Foster, L. J. & Duong Van Hoa, F.
1181 Profiling the Escherichia coli membrane protein interactome captured in
1182 Peptidisc libraries. *eLife* **8**, doi:10.7554/eLife.46615 (2019).
1183 48 Alvira, S., Watkins, D. W., Troman, L., Allen, W. J., Lorriman, J.,
1184 Degliesposti, G., Cohen, E. J., Beeby, M., Daum, B., Gold, V. A. M., Skehel,
1185 J. M. & Collinson, I. Inter-membrane association of the Sec and BAM
1186 translocons for bacterial outer-membrane biogenesis. *bioRxiv*, 589077,
1187 doi:10.1101/589077 (2020).
1188 49 Li, G. W., Burkhardt, D., Gross, C. & Weissman, J. S. Quantifying absolute
1189 protein synthesis rates reveals principles underlying allocation of cellular
1190 resources. *Cell* **157**, 624-635, doi:10.1016/j.cell.2014.02.033 (2014).
1191 50 Nakamura, K. & Mizushima, S. Effects of heating in dodecyl sulfate solution
1192 on the conformation and electrophoretic mobility of isolated major outer
1193 membrane proteins from Escherichia coli K-12. *Journal of biochemistry* **80**,
1194 1411-1422, doi:10.1093/oxfordjournals.jbchem.a131414 (1976).
1195 51 Rouviere, P. E. & Gross, C. A. SurA, a periplasmic protein with peptidyl-prolyl
1196 isomerase activity, participates in the assembly of outer membrane porins.
1197 *Genes & development* **10**, 3170-3182, doi:10.1101/gad.10.24.3170 (1996).
1198 52 Charlson, E. S., Werner, J. N. & Misra, R. Differential effects of yfgL mutation
1199 on Escherichia coli outer membrane proteins and lipopolysaccharide. *Journal*
1200 *of bacteriology* **188**, 7186-7194, doi:10.1128/jb.00571-06 (2006).
1201 53 Guo, M. S., Updegrove, T. B., Gogol, E. B., Shabalina, S. A., Gross, C. A. &
1202 Storz, G. MicL, a new σE-dependent sRNA, combats envelope stress by
1203 repressing synthesis of Lpp, the major outer membrane lipoprotein. *Genes &*
1204 *development* **28**, 1620-1634, doi:10.1101/gad.243485.114 (2014).
1205 54 Gogol, E. B., Rhodius, V. A., Papenfort, K., Vogel, J. & Gross, C. A. Small
1206 RNAs endow a transcriptional activator with essential repressor functions for

1207 single-tier control of a global stress regulon. *Proceedings of the National*
1208 *Academy of Sciences of the United States of America* **108**, 12875-12880,
1209 doi:10.1073/pnas.1109379108 (2011).
1210 55 Roman-Hernandez, G., Peterson, J. H. & Bernstein, H. D. Reconstitution of
1211 bacterial autotransporter assembly using purified components. *eLife* **3**,
1212 e04234, doi:10.7554/eLife.04234 (2014).
1213 56 Hale, C. A. & de Boer, P. A. Direct binding of FtsZ to ZipA, an essential
1214 component of the septal ring structure that mediates cell division in E. coli.
1215 *Cell* **88**, 175-185, doi:10.1016/s0092-8674(00)81838-3 (1997).
1216 57 Hartmann, J. B., Zahn, M., Burmann, I. M., Bibow, S. & Hiller, S. Sequence-
1217 Specific Solution NMR Assignments of the beta-Barrel Insertase BamA to
1218 Monitor Its Conformational Ensemble at the Atomic Level. *Journal of the*
1219 *American Chemical Society* **140**, 11252-11260, doi:10.1021/jacs.8b03220
1220 (2018).
1221 58 Vertommen, D., Ruiz, N., Leverrier, P., Silhavy, T. J. & Collet, J. F.
1222 Characterization of the role of the Escherichia coli periplasmic chaperone
1223 SurA using differential proteomics. *Proteomics* **9**, 2432-2443,
1224 doi:10.1002/pmic.200800794 (2009).
1225 59 Konovalova, A., Schwalm, J. A. & Silhavy, T. J. A Suppressor Mutation That
1226 Creates a Faster and More Robust sigmaE Envelope Stress Response.
1227 *Journal of bacteriology* **198**, 2345-2351, doi:10.1128/jb.00340-16 (2016).
1228 60 Kern, B., Leiser, O. P. & Misra, R. Suppressor Mutations in degS Overcome
1229 the Acute Temperature-Sensitive Phenotype of DeltadegP and DeltadegP
1230 Deltatol-pal Mutants of Escherichia coli. *Journal of bacteriology* **201**,
1231 doi:10.1128/jb.00742-18 (2019).
1232 61 Hart, E. M., O'Connell, A., Tang, K., Wzorek, J. S., Grabowicz, M., Kahne, D.
1233 & Silhavy, T. J. Fine-Tuning of sigma(E) Activation Suppresses Multiple
1234 Assembly-Defective Mutations in Escherichia coli. *Journal of bacteriology*
1235 **201**, doi:10.1128/jb.00745-18 (2019).
1236 62 Leiser, O. P., Charlson, E. S., Gerken, H. & Misra, R. Reversal of the ΔdegP
1237 phenotypes by a novel rpoE allele of Escherichia coli. *PloS one* **7**, e33979,
1238 doi:10.1371/journal.pone.0033979 (2012).
1239 63 Yeats, C. & Bateman, A. The BON domain: a putative membrane-binding
1240 domain. *Trends in biochemical sciences* **28**, 352-355, doi:10.1016/s0968-
1241 0004(03)00115-4 (2003).
1242 64 Bryant, J. A., Morris, F. C., Knowles, T. J., Maderbocus, R., Heinz, E.,
1243 Boelter, G., Alodaini, D., Colyer, A., Wotherspoon, P. J., Staunton, K. A.,
1244 Jeeves, M., Browning, D. F., Sevastsyanovich, Y. R., Wells, T. J., Rossiter,
1245 A. E., Bavro, V. N., Sridhar, P., Ward, D. G., Chong, Z. S., Icke, C., Teo, A.,
1246 Chng, S. S., Roper, D. I., Lithgow, T., Cunningham, A. F., Banzhaf, M.,
1247 Overduin, M. & Henderson, I. R. Structure-function analyses of dual-BON
1248 domain protein DolP identifies phospholipid binding as a new mechanism for
1249 protein localisation. *bioRxiv*, 2020.2008.2010.244616,
1250 doi:10.1101/2020.08.10.244616 (2020).
1251 65 Fleming, K. G. A combined kinetic push and thermodynamic pull as driving
1252 forces for outer membrane protein sorting and folding in bacteria.
1253 *Philosophical transactions of the Royal Society of London. Series B,*
1254 *Biological sciences* **370**, doi:10.1098/rstb.2015.0026 (2015).
1255 66 Horne, J. E., Brockwell, D. J. & Radford, S. E. Role of the lipid bilayer in
1256 outer membrane protein folding in Gram-negative bacteria. *The Journal of*

biological chemistry **295**, 10340-10367, doi:10.1074/jbc.REV120.011473 (2020).

67 Sinnige, T., Weingarth, M., Renault, M., Baker, L., Tommassen, J. & Baldus, M. Solid-state NMR studies of full-length BamA in lipid bilayers suggest limited overall POTRA mobility. *Journal of molecular biology* **426**, 2009-2021, doi:10.1016/j.jmb.2014.02.007 (2014).

68 Rassam, P., Copeland, N. A., Birkholz, O., Tóth, C., Chavent, M., Duncan, A. L., Cross, S. J., Housden, N. G., Kaminska, R., Seger, U., Quinn, D. M., Garrod, T. J., Sansom, M. S., Piehler, J., Baumann, C. G. & Kleanthous, C. Supramolecular assemblies underpin turnover of outer membrane proteins in bacteria. *Nature* **523**, 333-336, doi:10.1038/nature14461 (2015).

69 Gunasinghe, S. D., Shiota, T., Stubenrauch, C. J., Schulze, K. E., Webb, C. T., Fulcher, A. J., Dunstan, R. A., Hay, I. D., Naderer, T., Whelan, D. R., Bell, T. D. M., Elgass, K. D., Strugnell, R. A. & Lithgow, T. The WD40 Protein BamB Mediates Coupling of BAM Complexes into Assembly Precincts in the Bacterial Outer Membrane. *Cell reports* **23**, 2782-2794, doi:10.1016/j.celrep.2018.04.093 (2018).

70 Jarosławski, S., Duquesne, K., Sturgis, J. N. & Scheuring, S. High-resolution architecture of the outer membrane of the Gram-negative bacteria Roseobacter denitrificans. *Molecular microbiology* **74**, 1211-1222, doi:10.1111/j.1365-2958.2009.06926.x (2009).

71 Lessen, H. J., Fleming, P. J., Fleming, K. G. & Sodt, A. J. Building Blocks of the Outer Membrane: Calculating a General Elastic Energy Model for β-Barrel Membrane Proteins. *Journal of chemical theory and computation* **14**, 4487-4497, doi:10.1021/acs.jctc.8b00377 (2018).

72 Cascales, E., Bernadac, A., Gavioli, M., Lazzaroni, J. C. & Lloubes, R. Pal lipoprotein of Escherichia coli plays a major role in outer membrane integrity. *Journal of bacteriology* **184**, 754-759, doi:10.1128/jb.184.3.754-759.2002 (2002).

73 Asmar, A. T. & Collet, J. F. Lpp, the Braun lipoprotein, turns 50-major achievements and remaining issues. *FEMS microbiology letters* **365**, doi:10.1093/femsle/fny199 (2018).

74 Grenier, F., Matteau, D., Baby, V. & Rodrigue, S. Complete Genome Sequence of Escherichia coli BW25113. *Genome announcements* **2**, doi:10.1128/genomeA.01038-14 (2014).

75 Blattner, F. R., Plunkett, G., 3rd, Bloch, C. A., Perna, N. T., Burland, V., Riley, M., Collado-Vides, J., Glasner, J. D., Rode, C. K., Mayhew, G. F., Gregor, J., Davis, N. W., Kirkpatrick, H. A., Goeden, M. A., Rose, D. J., Mau, B. & Shao, Y. The complete genome sequence of Escherichia coli K-12. *Science (New York, N.Y.)* **277**, 1453-1462, doi:10.1126/science.277.5331.1453 (1997).

76 Datsenko, K. A. & Wanner, B. L. One-step inactivation of chromosomal genes in Escherichia coli K-12 using PCR products. *Proceedings of the National Academy of Sciences of the United States of America* **97**, 6640-6645, doi:10.1073/pnas.120163297 (2000).

77 Knop, M., Siegers, K., Pereira, G., Zachariae, W., Winsor, B., Nasmyth, K. & Schiebel, E. Epitope tagging of yeast genes using a PCR-based strategy: more tags and improved practical routines. *Yeast (Chichester, England)* **15**, 963-972, doi:10.1002/(sici)1097-0061(199907)15:10b<963::Aid-yea399>3.0.Co;2-w (1999).

78 McLeay, R. C. & Bailey, T. L. Motif Enrichment Analysis: a unified framework and an evaluation on ChIP data. *BMC bioinformatics* **11**, 165, doi:10.1186/1471-2105-11-165 (2010).

79 Ieva, R. & Bernstein, H. D. Interaction of an autotransporter passenger domain with BamA during its translocation across the bacterial outer membrane. *Proceedings of the National Academy of Sciences of the United States of America* **106**, 19120-19125, doi:10.1073/pnas.0907912106 (2009).

80 Vischer, N. O., Verheul, J., Postma, M., van den Berg van Saparoea, B., Galli, E., Natale, P., Gerdes, K., Luirink, J., Vollmer, W., Vicente, M. & den Blaauwen, T. Cell age dependent concentration of Escherichia coli divisome proteins analyzed with ImageJ and ObjectJ. *Frontiers in microbiology* **6**, 586, doi:10.3389/fmicb.2015.00586 (2015).

81 Ashburner, M., Ball, C. A., Blake, J. A., Botstein, D., Butler, H., Cherry, J. M., Davis, A. P., Dolinski, K., Dwight, S. S., Eppig, J. T., Harris, M. A., Hill, D. P., Issel-Tarver, L., Kasarskis, A., Lewis, S., Matese, J. C., Richardson, J. E., Ringwald, M., Rubin, G. M. & Sherlock, G. Gene ontology: tool for the unification of biology. The Gene Ontology Consortium. *Nature genetics* **25**, 25-29, doi:10.1038/75556 (2000).

82 Albenne, C. & Ieva, R. Job contenders: roles of the beta-barrel assembly machinery and the translocation and assembly module in autotransporter secretion. *Molecular microbiology* **106**, 505-517, doi:10.1111/mmi.13832 (2017).

83 Szabady, R. L., Peterson, J. H., Skillman, K. M. & Bernstein, H. D. An unusual signal peptide facilitates late steps in the biogenesis of a bacterial autotransporter. *Proceedings of the National Academy of Sciences of the United States of America* **102**, 221-226, doi:10.1073/pnas.0406055102 (2005).

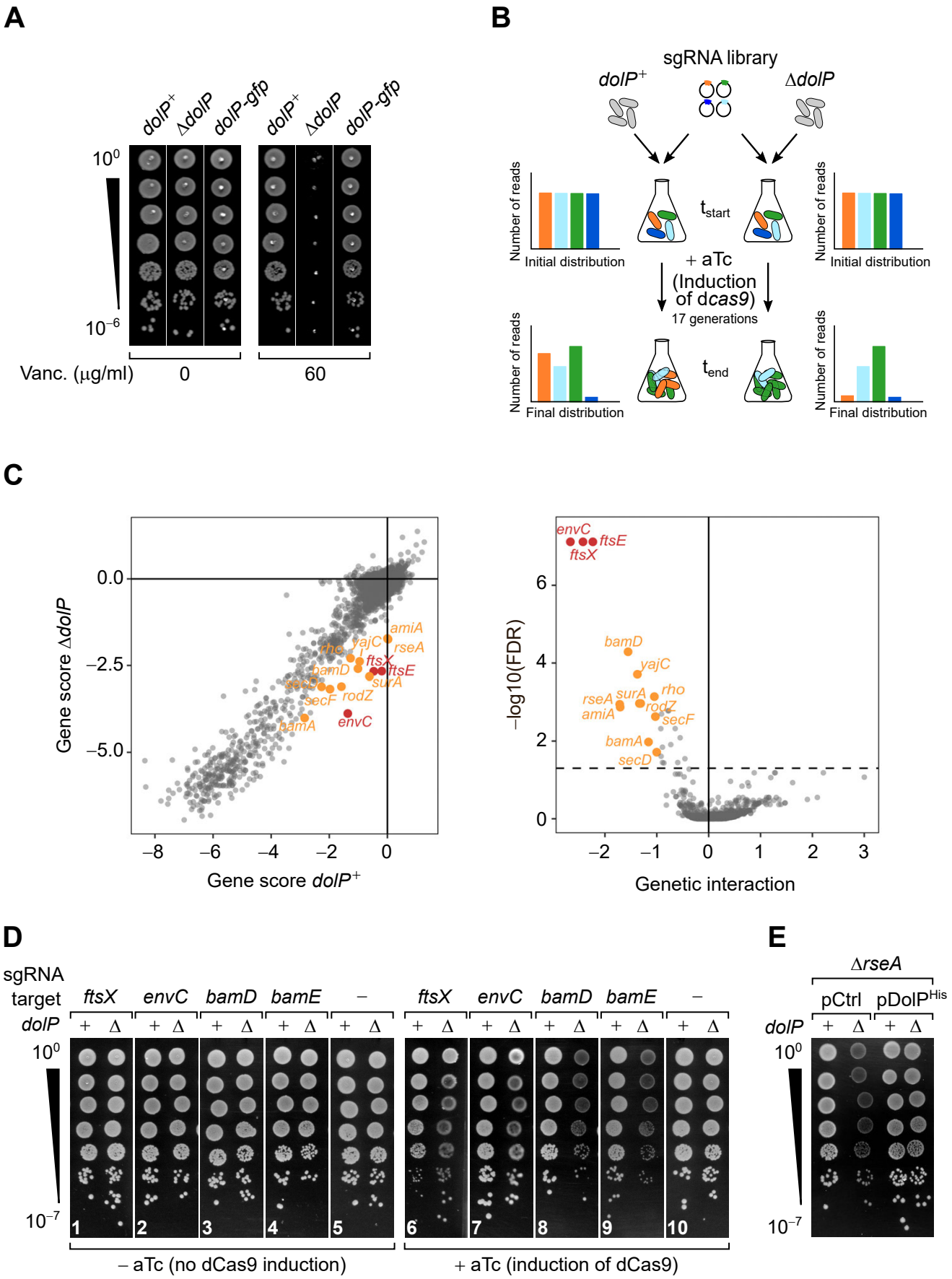
A
dolP+
ΔdolP
dolP-gfp
dolP+
ΔdolP
dolP-gfp
10^0
10^−6
Vanc. (μg/ml)
0
60
B
sgRNA library
dolP+
ΔdolP
Number of reads
Initial distribution
t_start
+ aTc
(Induction of dcas9)
17 generations
t_end
Final distribution
C
Gene score ΔdolP
Gene score dolP+
amiA
rseA
yajC
rho
ftsX
ftsE
bamD
secD
surA
secF
rodZ
bamA
envC
−log10(FDR)
Genetic interaction
D
sgRNA target
ftsX
envC
bamD
bamE
–
dolP
+
Δ
10^0
10^−7
1
2
3
4
5
6
7
8
9
10
– aTc (no dCas9 induction)
+ aTc (induction of dCas9)
E
ΔrseA
pCtrl
pDolP^His
dolP
+
Δ
10^0
10^−7

Figure 1.

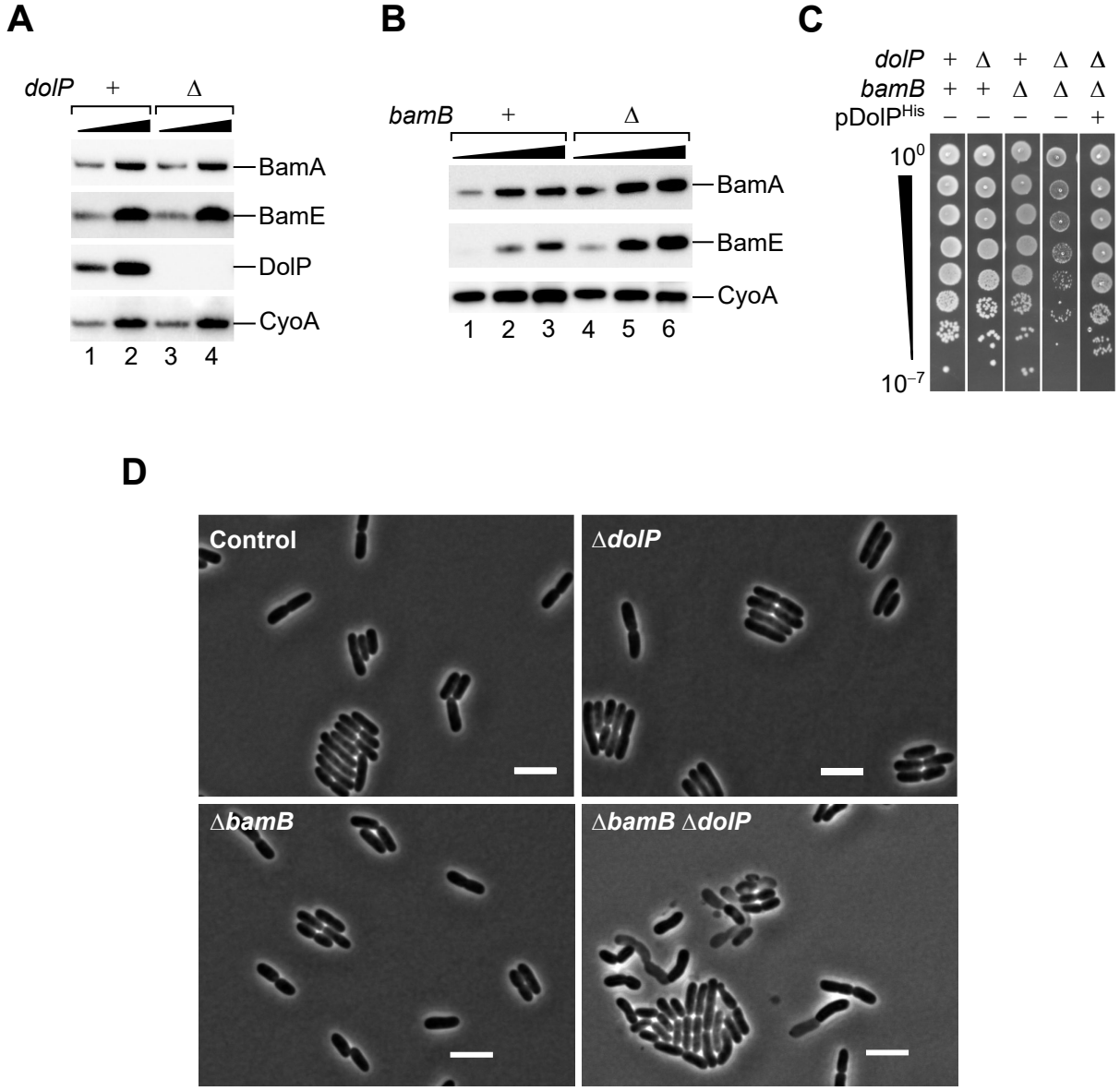
A
dolP + Δ
BamA
BamE
DolP
CyoA
1 2 3 4
B
bamB + Δ
BamA
BamE
CyoA
1 2 3 4 5 6
C
dolP + Δ + Δ Δ
bamB + + Δ Δ Δ
pDolP^His – – – – +
10^0
10^−7
D
Control
ΔdolP
ΔbamB
ΔbamB ΔdolP

Figure 2.

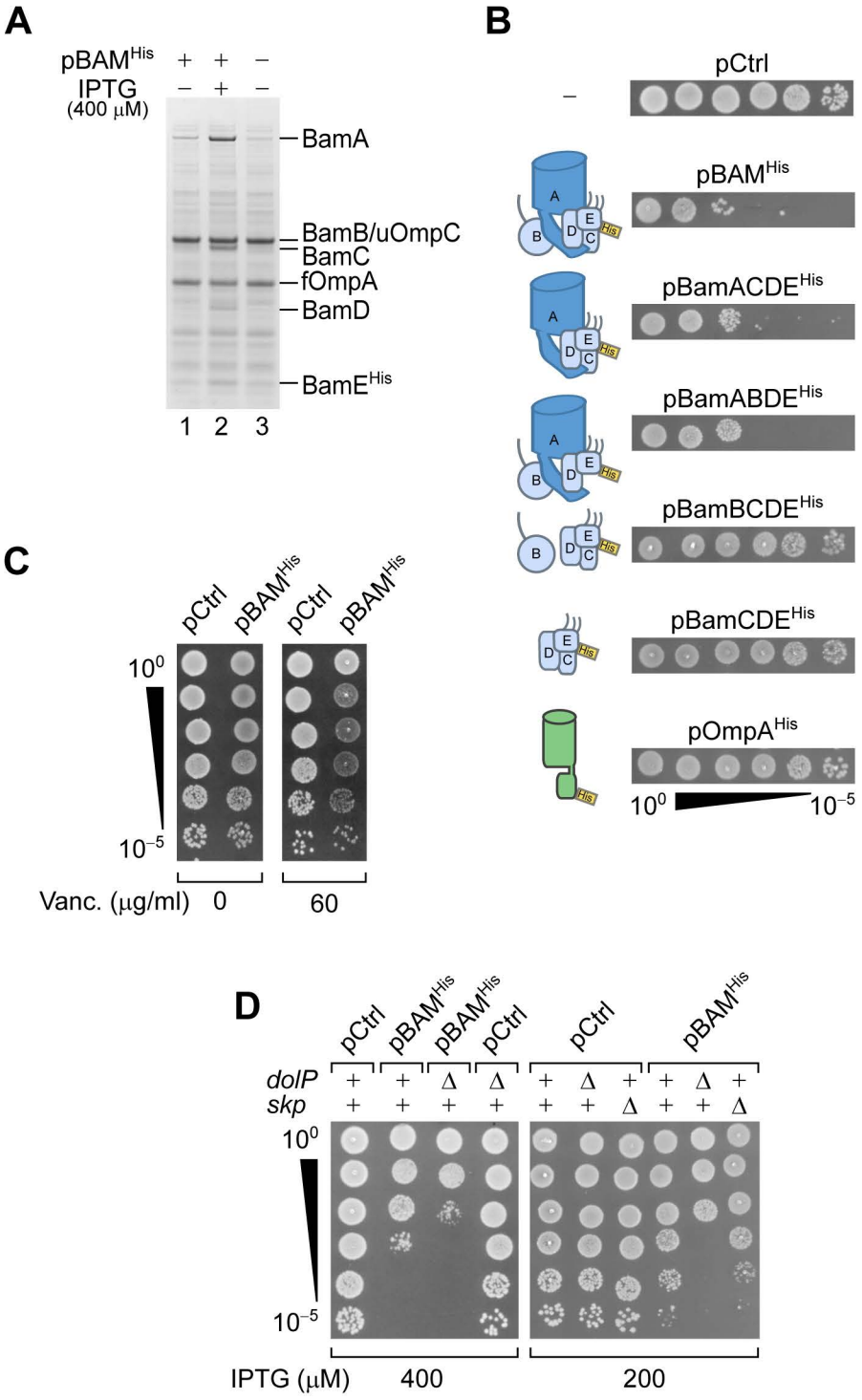
A
pBAM^His + + −
IPTG − + −
(400 μM)
BamA
BamB/uOmpC
BamC
fOmpA
BamD
BamE^His
1 2 3
B
pCtrl
pBAM^His
pBamACDE^His
pBamABDE^His
pBamBCDE^His
pBamCDE^His
pOmpA^His
10^0
10^−5
C
pCtrl
pBAM^His
pCtrl
pBAM^His
10^0
10^−5
Vanc. (μg/ml) 0 60
D
pCtrl
pBAM^His
pBAM^His
pCtrl
pCtrl
pBAM^His
dolP + + Δ Δ + Δ + + Δ +
skp + + + + + + Δ + + Δ
10^0
10^−5
IPTG (μM) 400 200

Figure 3.

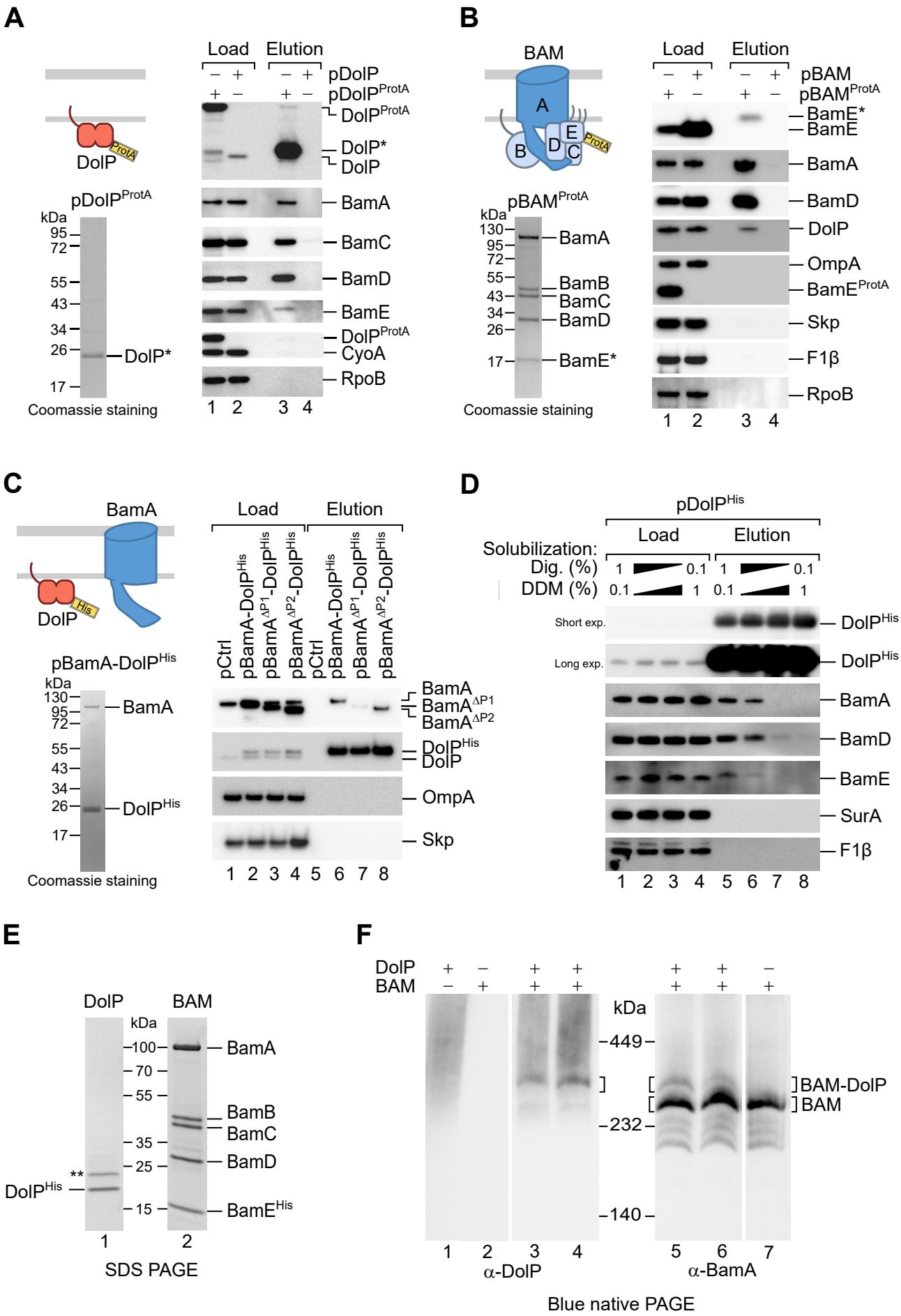
A
Load
Elution
pDolP
pDolP^ProtA
DolP^ProtA
DolP*
DolP
BamA
BamC
BamD
BamE
DolP^ProtA
CyoA
RpoB
DolP
ProtA
pDolP^ProtA
kDa
95
72
55
43
34
26
17
DolP*
Coomassie staining
1 2 3 4
B
BAM
A
B
C
D
E
ProtA
pBAM
pBAM^ProtA
BamE*
BamE
BamA
BamD
DolP
OmpA
BamE^ProtA
Skp
F1β
RpoB
pBAM^ProtA
kDa
130
95
72
55
43
34
26
17
BamA
BamB
BamC
BamD
BamE*
Coomassie staining
1 2 3 4
C
BamA
DolP
His
pBamA-DolP^His
Load
Elution
pCtrl
pBamA-DolP^His
pBamA^ΔP1-DolP^His
pBamA^ΔP2-DolP^His
BamA
BamA^ΔP1
BamA^ΔP2
DolP^His
DolP
OmpA
Skp
kDa
130
95
72
55
43
34
26
17
DolP^His
Coomassie staining
1 2 3 4 5 6 7 8
D
pDolP^His
Load
Elution
Solubilization:
Dig. (%)
DDM (%)
Short exp.
Long exp.
DolP^His
BamA
BamD
BamE
SurA
F1β
1 2 3 4 5 6 7 8
E
DolP
BAM
kDa
100
70
55
35
25
15
BamA
BamB
BamC
BamD
BamE^His
DolP^His
**
1 2
SDS PAGE
F
DolP
BAM
kDa
449
232
140
BAM-DolP
BAM
1 2 3 4
α-DolP
5 6 7
α-BamA
Blue native PAGE

Figure 4.

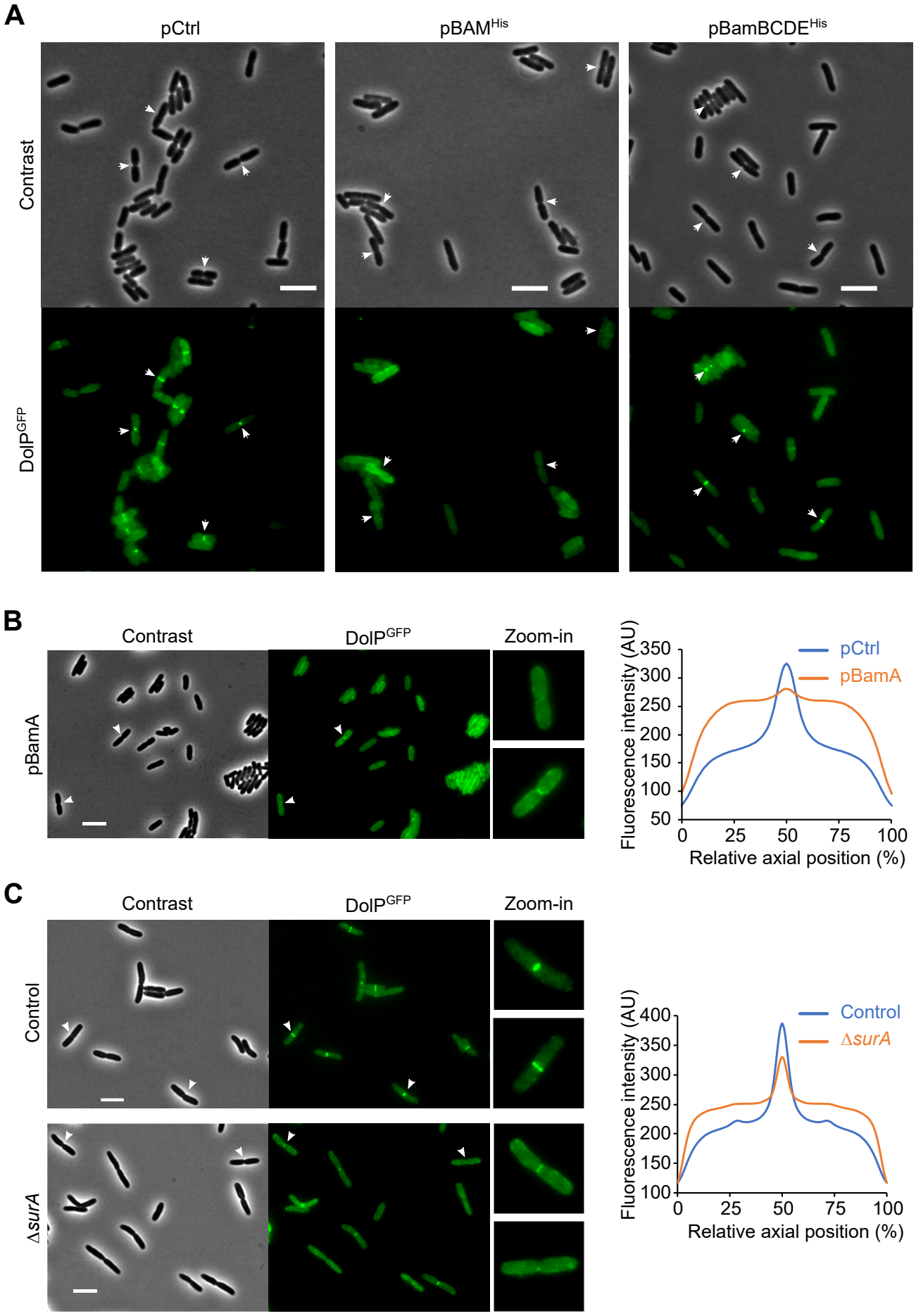
A
pCtrl
pBAM^His
pBamBCDE^His
Contrast
DolP^GFP
B
Contrast
DolP^GFP
Zoom-in
pBamA
Fluorescence intensity (AU)
350
300
250
200
150
100
50
0
25
50
75
100
Relative axial position (%)
pCtrl
pBamA
C
Contrast
DolP^GFP
Zoom-in
Control
ΔsurA
Fluorescence intensity (AU)
400
350
300
250
200
150
100
0
25
50
75
100
Relative axial position (%)
Control
ΔsurA

Figure 5.

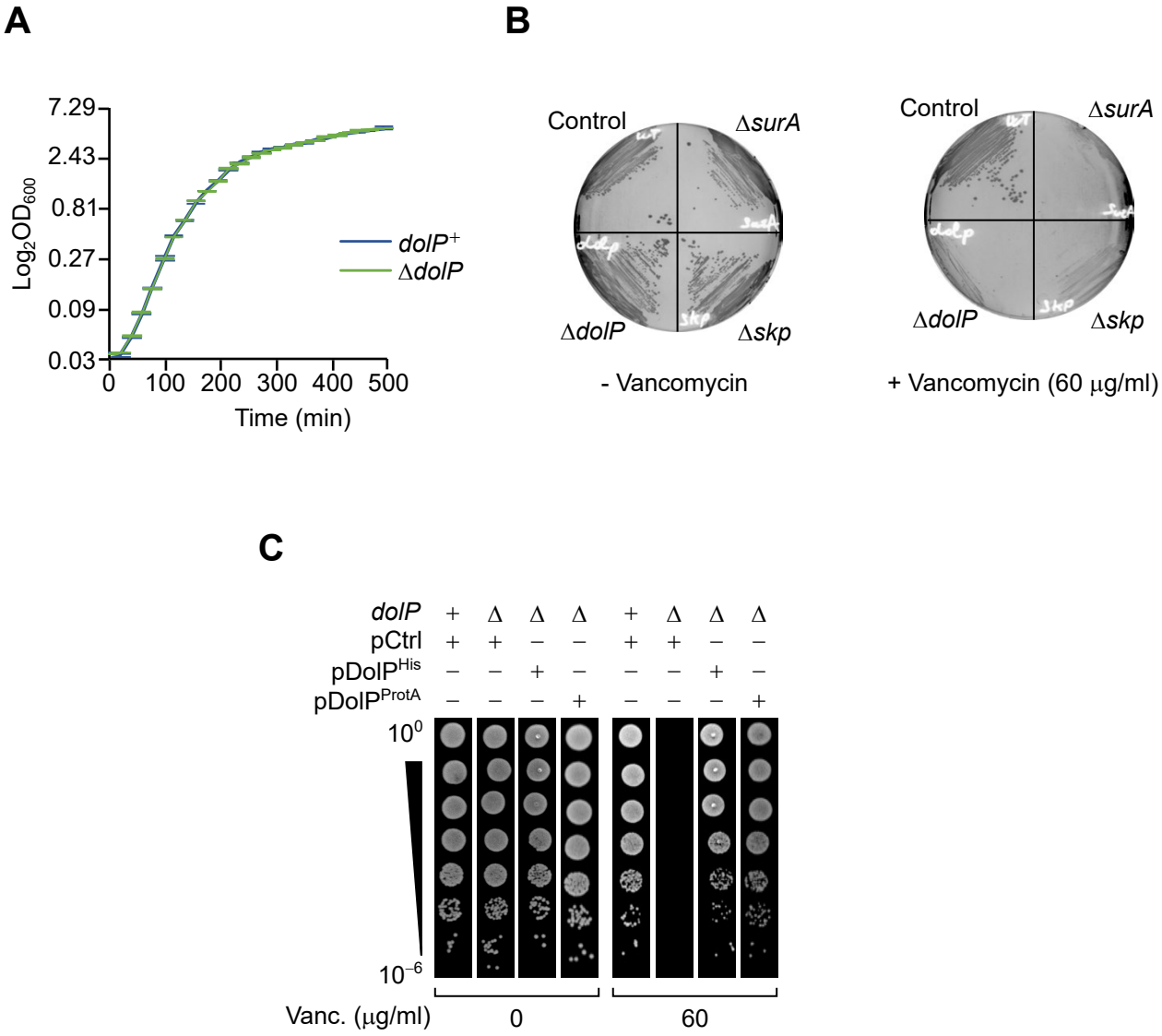
A
7.29
2.43
0.81
0.27
0.09
0.03
Log2OD600
0
100
200
300
400
500
Time (min)
dolP+
ΔdolP
B
Control
ΔsurA
ΔdolP
Δskp
- Vancomycin
Control
ΔsurA
ΔdolP
Δskp
+ Vancomycin (60 μg/ml)
C
dolP + Δ Δ Δ + Δ Δ Δ
pCtrl + + – – + + – –
pDolPHis – – + – – – + –
pDolPProtA – – – + – – – +
10^0
10^–6
Vanc. (μg/ml)
0
60

Figure S1.

A

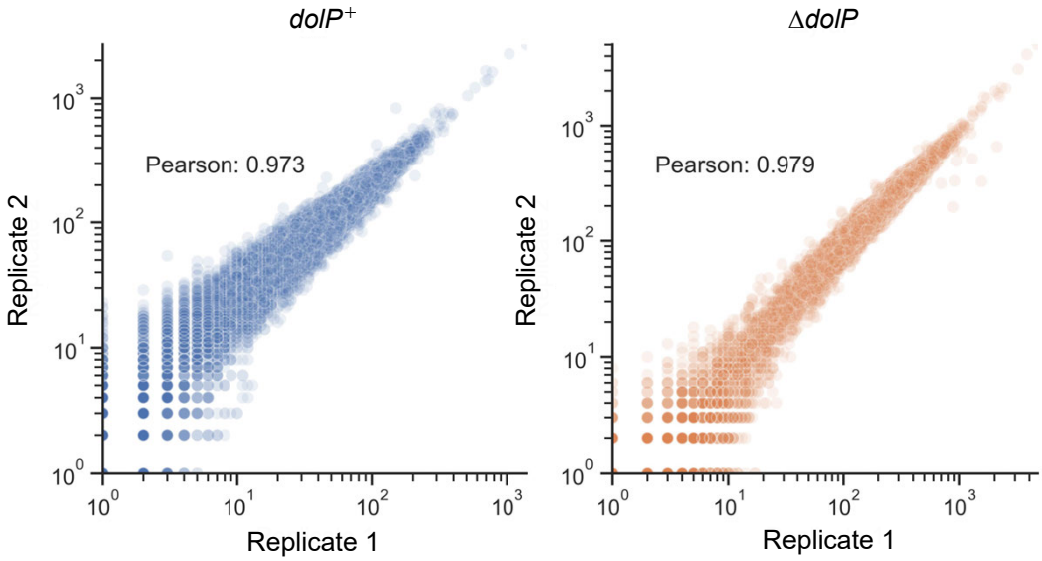

B

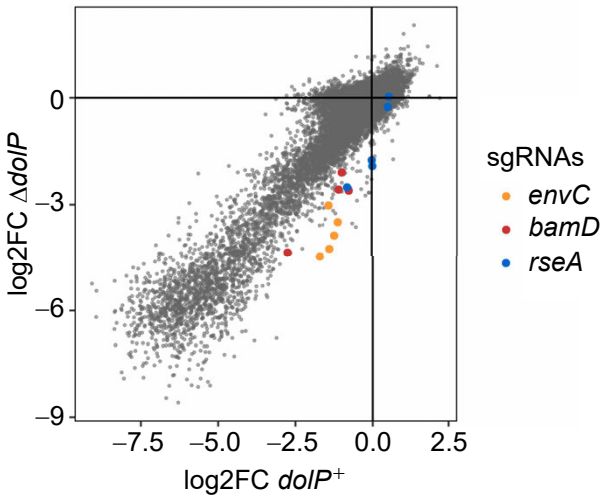

C

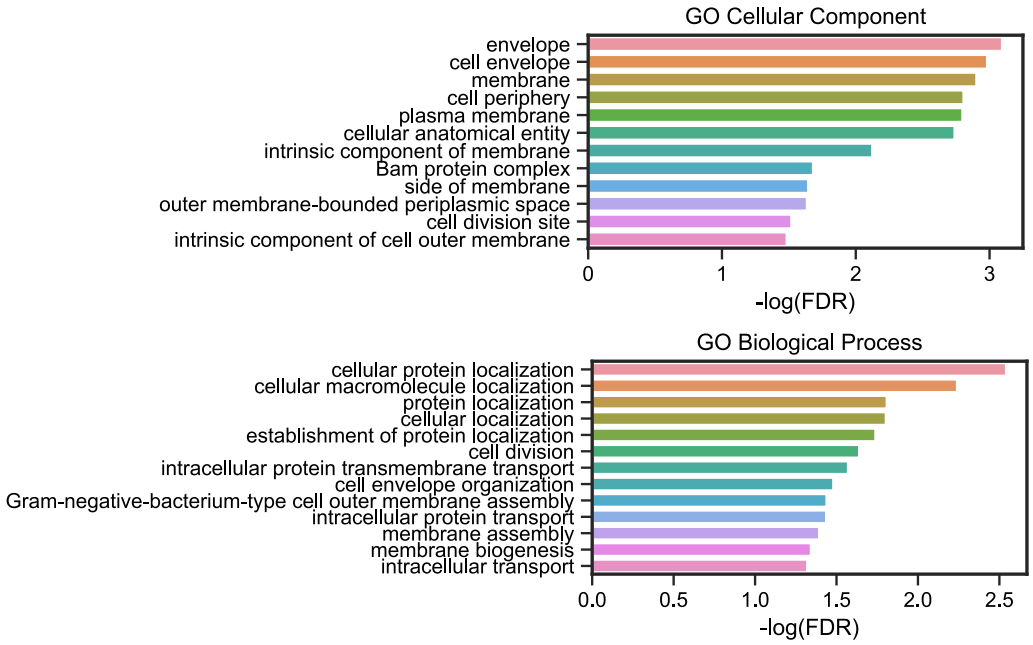

Figure S2.

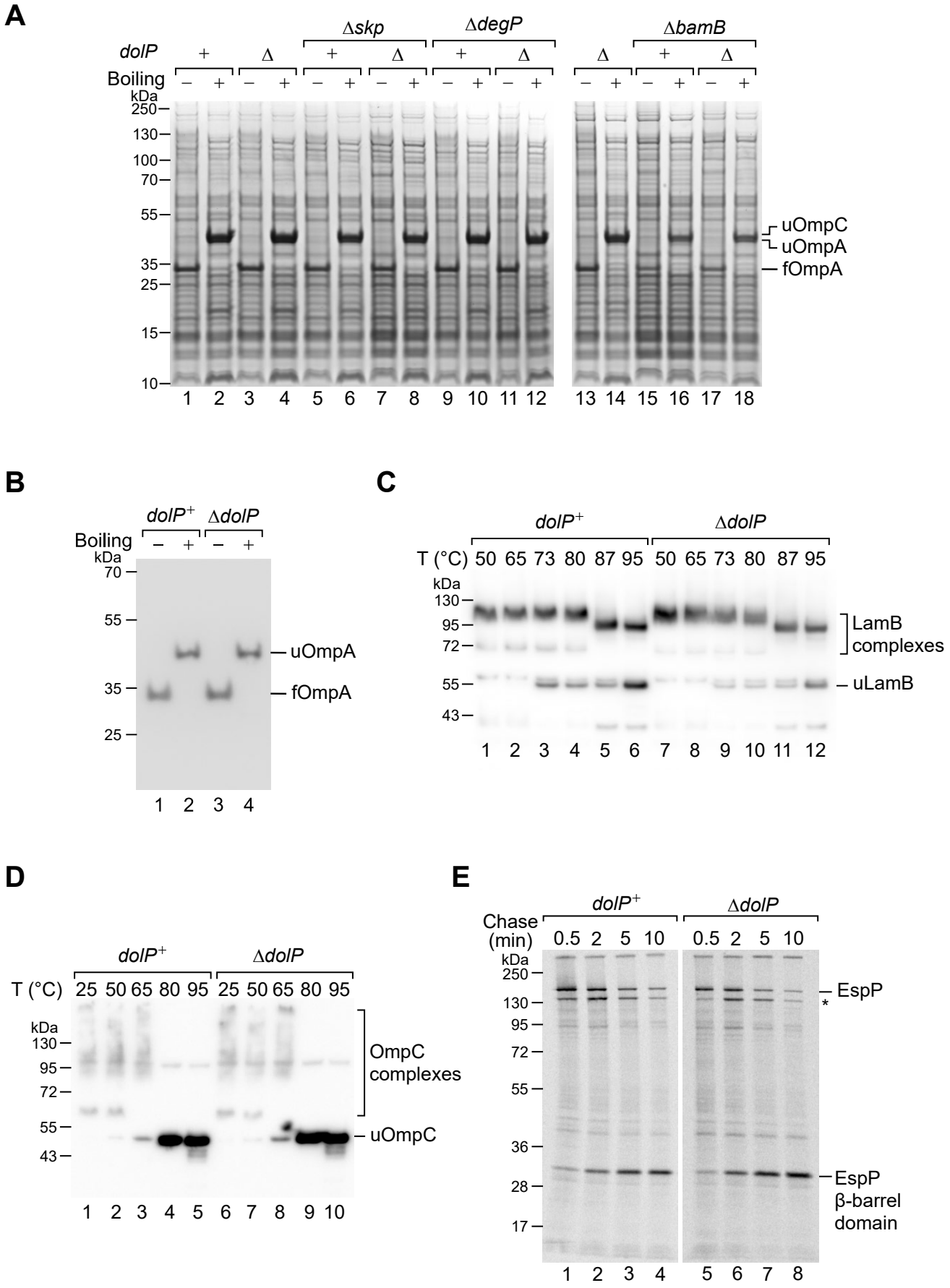
A
Δskp
ΔdegP
ΔbamB
dolP
+
Δ
Boiling
kDa
250
130
100
70
55
35
25
15
10
uOmpC
uOmpA
fOmpA
1 2 3 4 5 6 7 8 9 10 11 12 13 14 15 16 17 18
B
dolP+
ΔdolP
uOmpA
fOmpA
1 2 3 4
C
T (°C) 50 65 73 80 87 95 50 65 73 80 87 95
130
95
72
55
43
LamB complexes
uLamB
1 2 3 4 5 6 7 8 9 10 11 12
D
T (°C) 25 50 65 80 95 25 50 65 80 95
OmpC complexes
uOmpC
1 2 3 4 5 6 7 8 9 10
E
Chase (min) 0.5 2 5 10 0.5 2 5 10
250
130
95
72
55
36
28
17
EspP
*
EspP β-barrel domain
1 2 3 4 5 6 7 8

Figure S3.

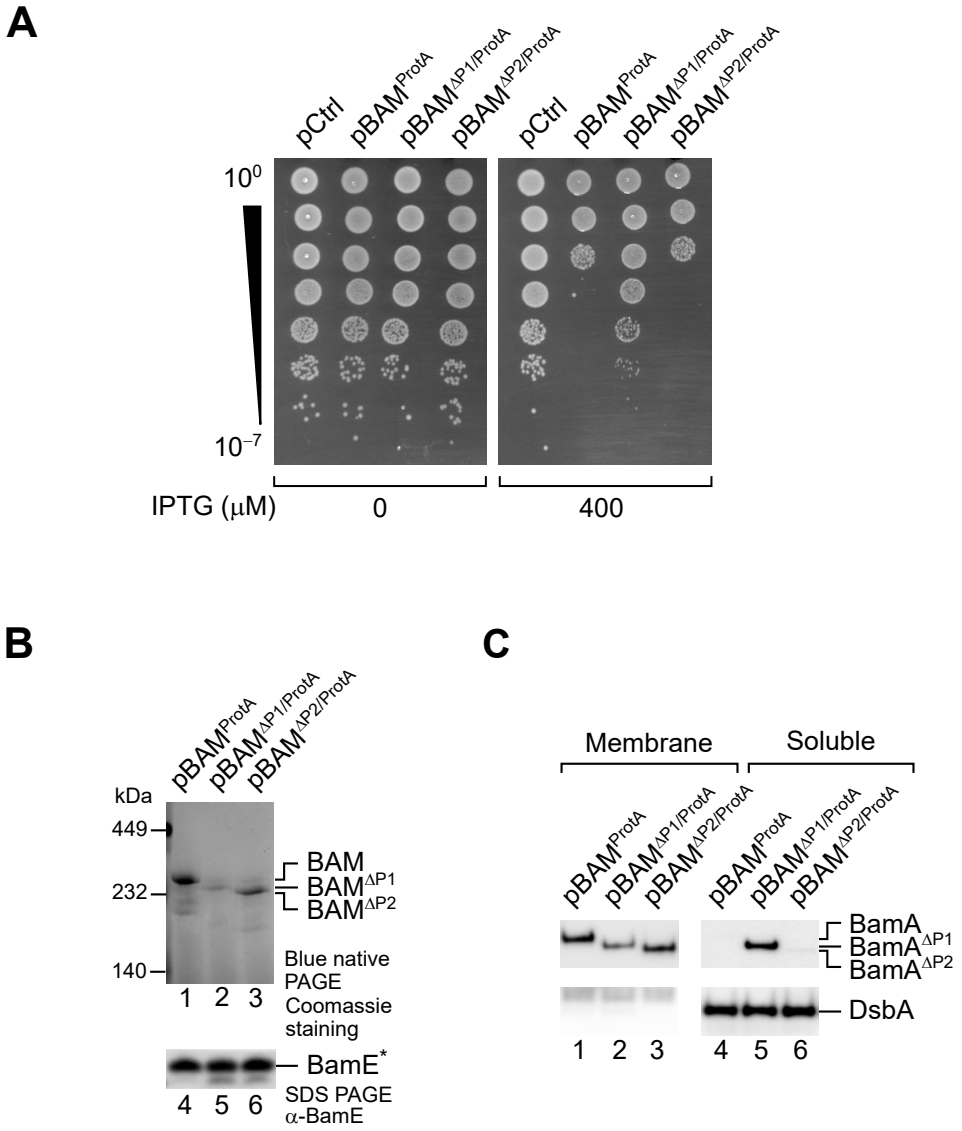
A
pCtrl
pBAM^ProtA
pBAM^ΔP1/ProtA
pBAM^ΔP2/ProtA
pCtrl
pBAM^ProtA
pBAM^ΔP1/ProtA
pBAM^ΔP2/ProtA
10^0
10^−7
IPTG (μM)
0
400
B
pBAM^ProtA
pBAM^ΔP1/ProtA
pBAM^ΔP2/ProtA
kDa
449
232
140
BAM
BAM^ΔP1
BAM^ΔP2
Blue native PAGE
Coomassie staining
1 2 3
BamE*
SDS PAGE
α-BamE
4 5 6
C
Membrane
Soluble
pBAM^ProtA
pBAM^ΔP1/ProtA
pBAM^ΔP2/ProtA
pBAM^ProtA
pBAM^ΔP1/ProtA
pBAM^ΔP2/ProtA
BamA
BamA^ΔP1
BamA^ΔP2
DsbA
1 2 3
4 5 6

Figure S4.

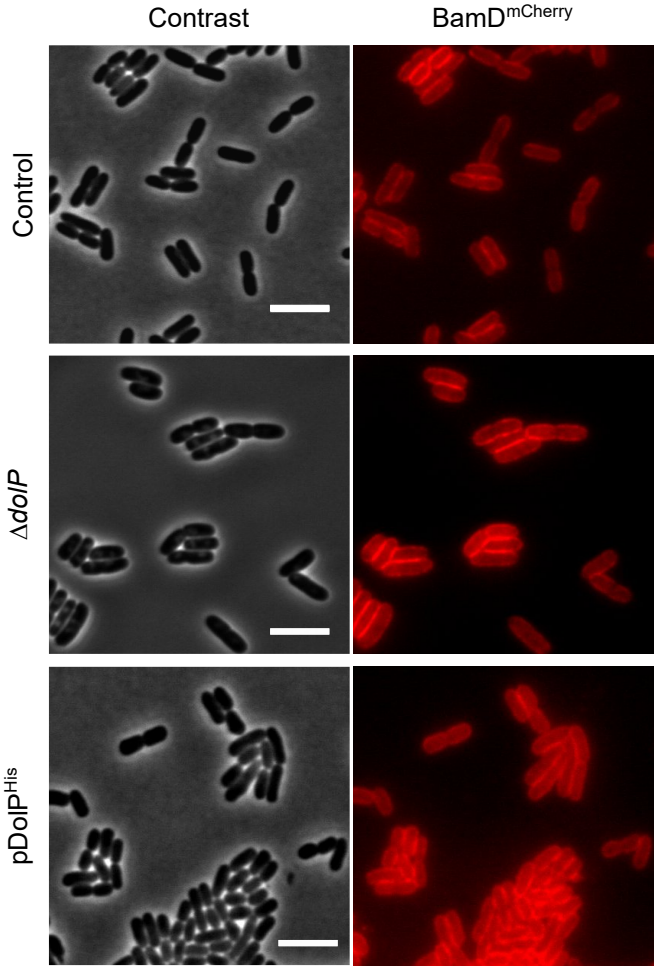

Figure S5.

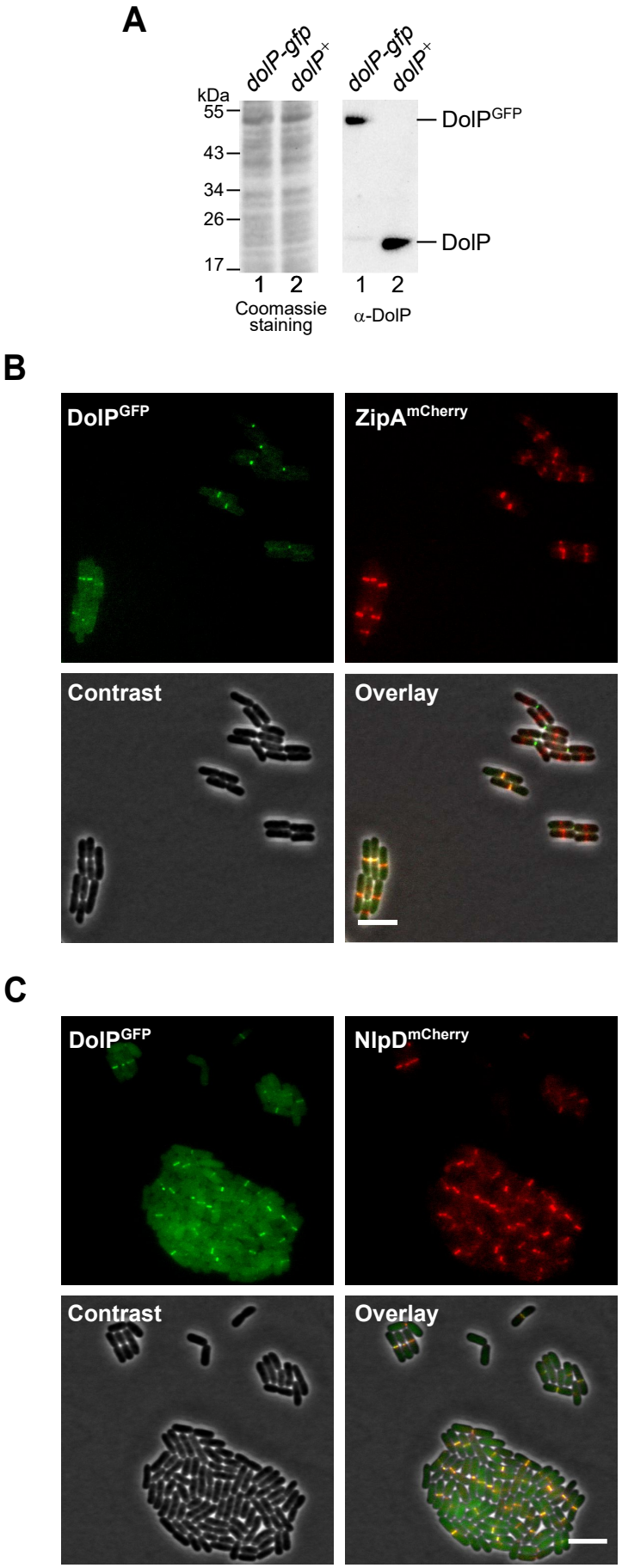
A
dolP-gfp
dolP+
dolP-gfp
dolP+
kDa
55
43
34
26
17
DolPGFP
DolP
1 2
Coomassie staining
1 2
α-DolP
B
DolPGFP
ZipAmCherry
Contrast
Overlay
C
DolPGFP
NlpDmCherry
Contrast
Overlay

Figure S6.

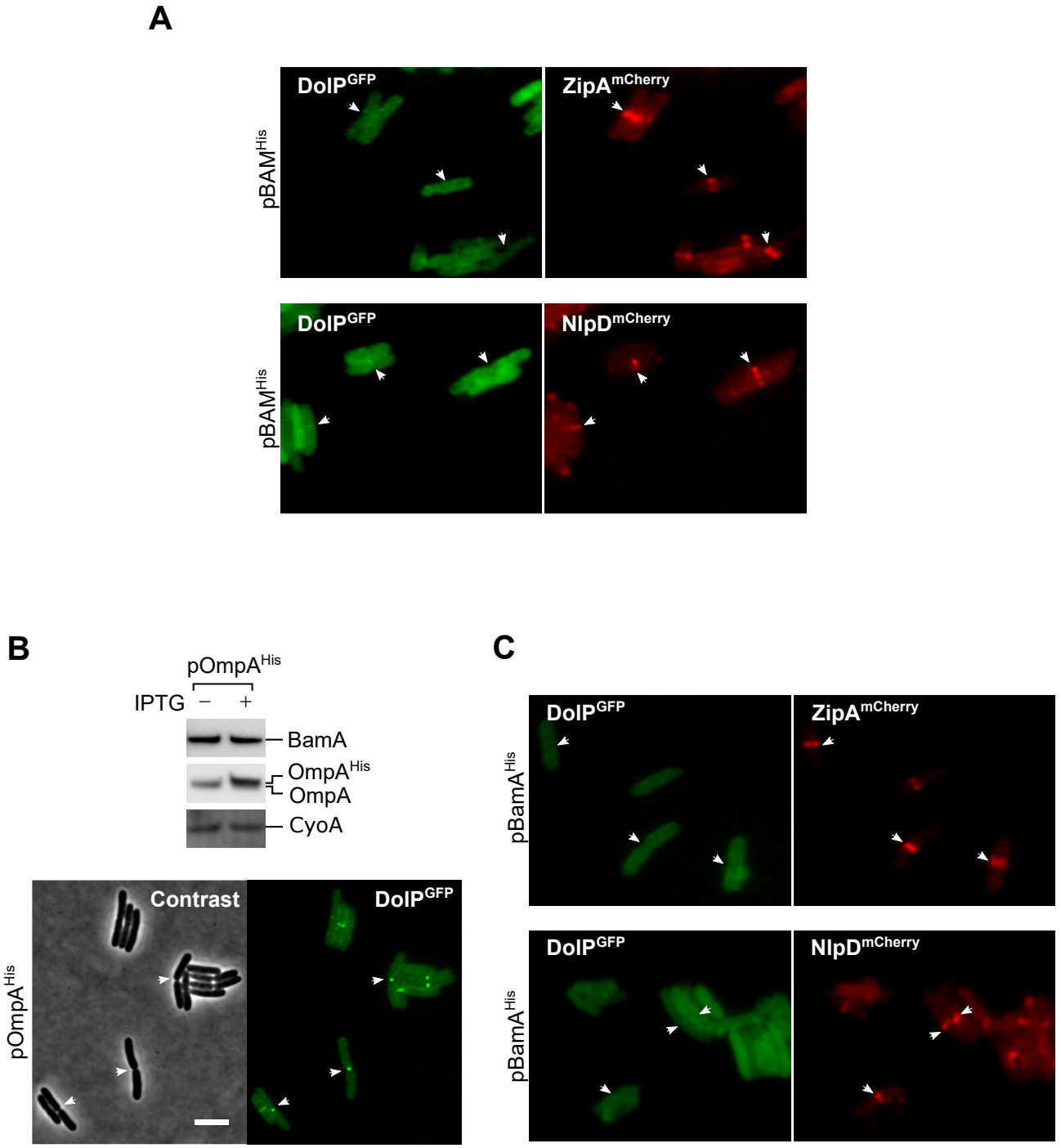
A
DolP^GFP
ZipA^mCherry
pBAM^His
DolP^GFP
NlpD^mCherry
pBAM^His
B
pOmpA^His
IPTG − +
BamA
OmpA^His
OmpA
CyoA
Contrast
DolP^GFP
pOmpA^His
C
DolP^GFP
ZipA^mCherry
pBamA^His
DolP^GFP
NlpD^mCherry
pBamA^His

Figure S7.

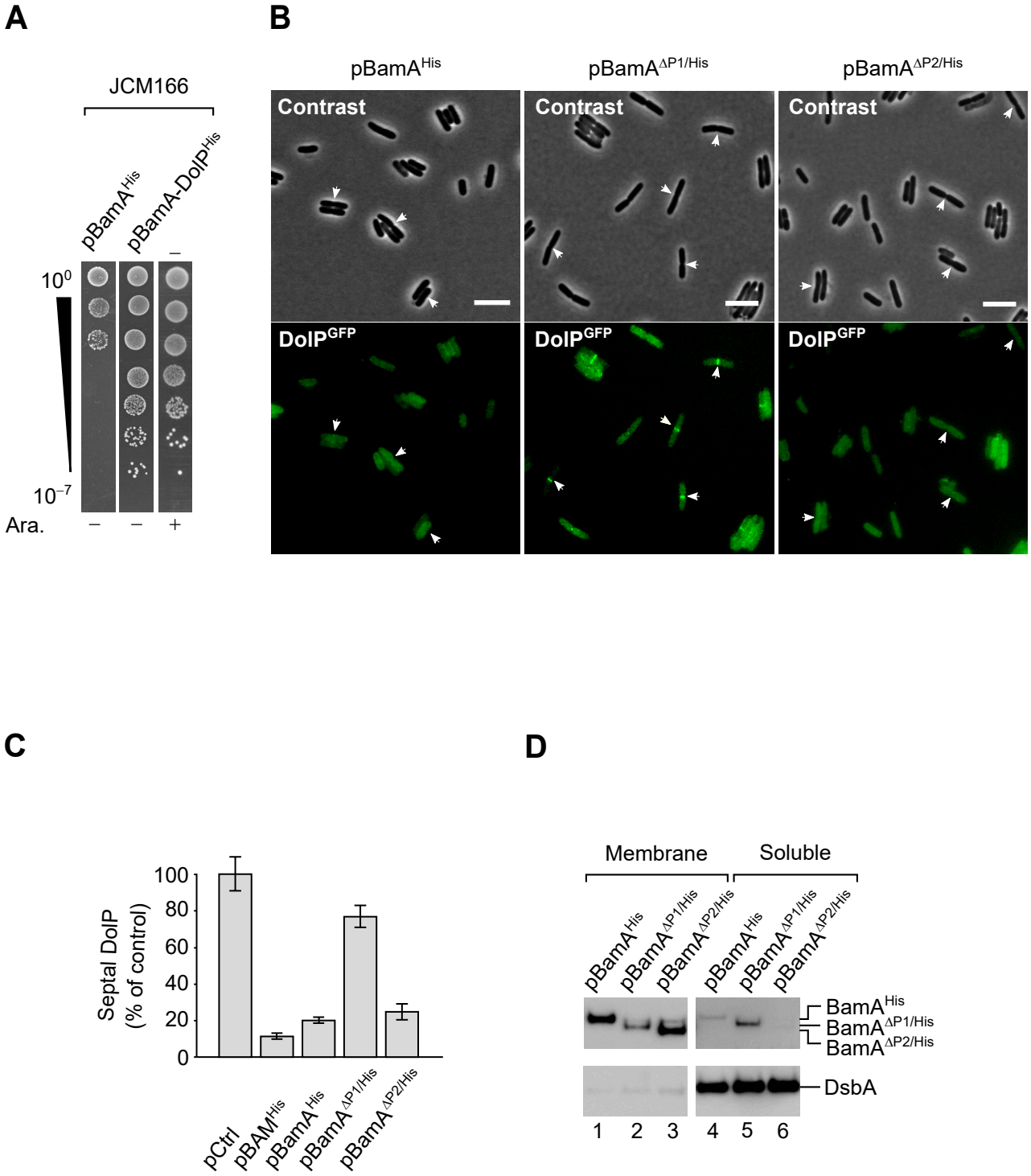
A
JCM166
pBamA^His
pBamA-DolP^His
–
10^0
10^–7
Ara.
–
–
+
B
pBamA^His
pBamA^ΔP1/His
pBamA^ΔP2/His
Contrast
Contrast
Contrast
DolP^GFP
DolP^GFP
DolP^GFP
C
Septal DolP
(% of control)
100
80
60
40
20
0
pCtrl
pBAM^His
pBamA^His
pBamA^ΔP1/His
pBamA^ΔP2/His
D
Membrane
Soluble
pBamA^His
pBamA^ΔP1/His
pBamA^ΔP2/His
pBamA^His
pBamA^ΔP1/His
pBamA^ΔP2/His
BamA^His
BamA^ΔP1/His
BamA^ΔP2/His
DsbA
1
2
3
4
5
6

Figure S8.

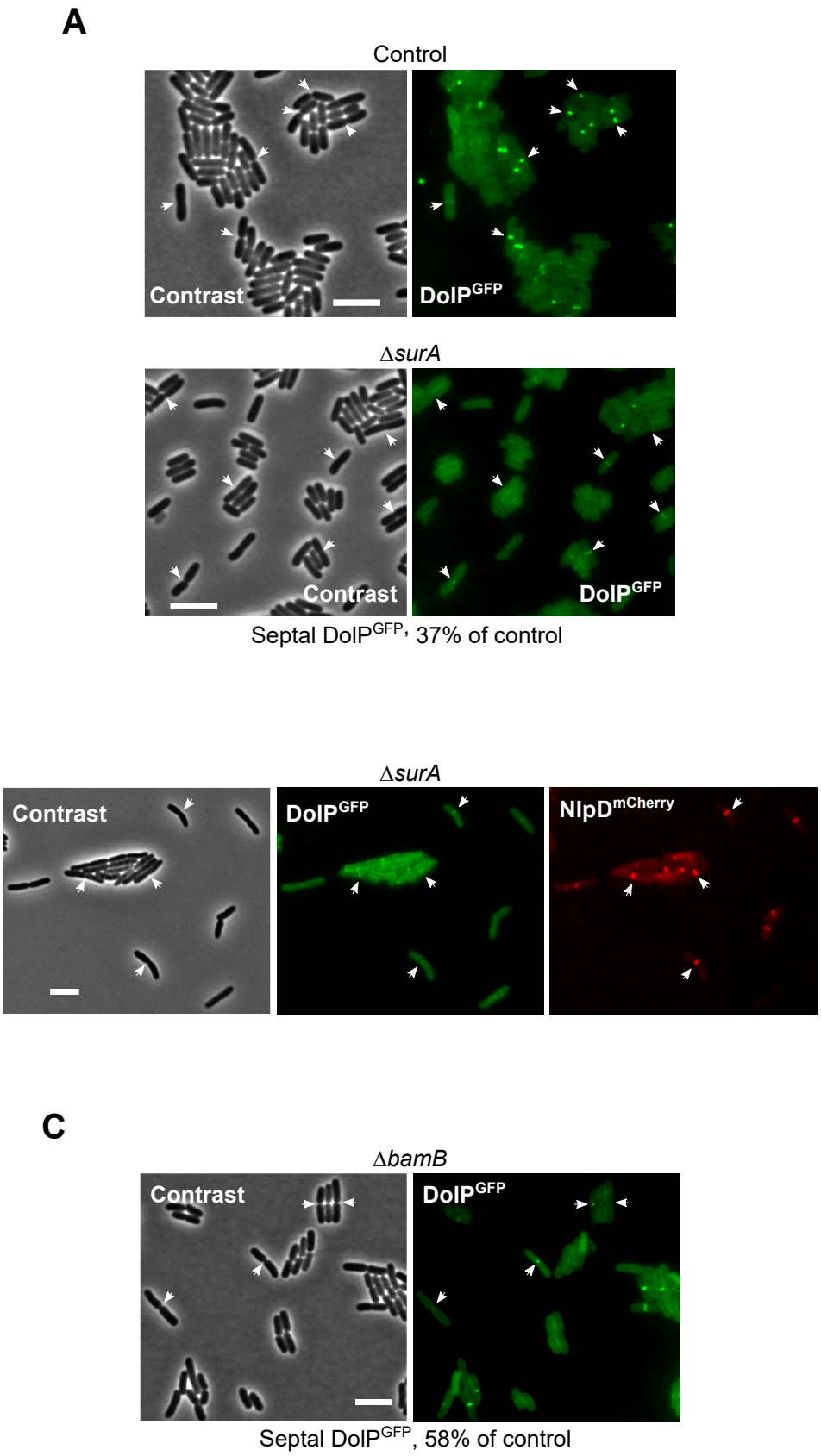
A
Control
Contrast
DolP^GFP
ΔsurA
Contrast
DolP^GFP
Septal DolP^GFP, 37% of control
B
ΔsurA
Contrast
DolP^GFP
NlpD^mCherry
C
ΔbamB
Contrast
DolP^GFP
Septal DolP^GFP, 58% of control

Figure S9.